EFFECT OF BROMOTRIFLUOROMETHANE AND TRIFLUOROMETHANE ON LAMINAR JET DIFFUSION FLAMES IN NORMAL AND MICROGRAVITY

by

Brad A. VanDerWege

B.S., Mechanical Engineering
University of Michigan, Ann Arbor
(1994)

Submitted to the Department of Mechanical Engineering
in Partial Fulfillment of the Requirements
for the Degree of

MASTER OF SCIENCE IN MECHANICAL ENGINEERING

AT THE

MASSACHUSETTS INSTITUTE OF TECHNOLOGY

February 1996

Signature of Author _____
Department of Mechanical Engineering
February 8, 1996

Certified by _____
Simone Hochgreb
Associate Professor of Mechanical Engineering
Thesis Supervisor

Accepted by _____
Ain A. Sonin
Chairman, Departmental Graduate Committee

EFFECT OF BROMOTRIFLUOROMETHANE AND TRIFLUOROMETHANE ON LAMINAR JET DIFFUSION FLAMES IN NORMAL AND MICROGRAVITY

by

Brad A. VanDerWege

Submitted to the Department of Mechanical Engineering
on January 19, 1996 in partial fulfillment
of the requirements for the Degree of
Master of Science in Mechanical Engineering.

ABSTRACT

The recent ban on the production of bromotrifluoromethane, because of its high stratospheric ozone depletion potential, has led to interest in finding an alternative agent for fire extinguishing applications. Fluorinated hydrocarbons are promising alternatives.

This work studies the effect of addition of the combustion inhibitors bromotrifluoromethane (CF_3Br) and trifluoromethane (CF_3H) to the oxidizing environment of laminar jet diffusion flames in normal gravity and microgravity. Experiments were performed at a range of oxygen concentrations, ambient pressures, fuel flow rates, and inhibitor concentration. Visual diagnostics were used to identify changes in structure and stability of the flames.

Addition of CF_3Br to the oxidizer environment was found to increase the soot luminosity and produce an orange- to red-colored luminous zone on the oxidizer side of the flame, possibly associated with inhibitor decomposition. Addition of CF_3H was found to decrease soot luminosity, but no decomposition zone could be observed. At high enough concentrations, the CF_3H-inhibited microgravity flame was blue and appeared to have an open tip. The limiting concentration of CF_3H required for flame extinction was found to be roughly twice as high on a mass basis and four times as high on a mole basis as CF_3Br. Soot luminosity was also found to increase with increasing fuel flow rate and increasing oxygen concentration. Flame tip opening, which is usually associated with soot formation, was observed for microgravity flames exhibiting no soot luminosity. The tendency for flame tip opening in microgravity was found to increase with decreasing fuel flow rate, decreasing oxygen concentration, and addition of inhibitors. Reduced pressure experiments at normal gravity showed that, although buoyancy effects are reduced, inhibitor effects are different than in microgravity.

Thesis Advisor: Prof. Simone Hochgreb
Associate Professor of Mechanical Engineering

ACKNOWLEDGMENTS

The guidance and dedication of Prof. Simone Hochgreb have made this work possible. Her accessibility and approachability have made her supervision dependable and welcome. The insight and expertise of Greg Linteris were a great asset in interpretation of the experiments. I thank Michael Bush for his help in getting this project going, despite his untimely departure.

I cannot thank David Urban enough for his invaluable assistance with the drop rig and preparations for the experiments. I am also grateful for the help of all the members of the drop tower crew at NASA-LeRC. In particular, I would like to thank Marlon Richmond for finding room for all the gasses I needed, Charles Traylor for all the extra drops I begged for, and Mike Johnston for the inspirational discussions on racing.

I would also like to thank Brian Corkum and Nancy Cook for the endless supply of tools, supplies, and purchase orders I required. The assistance of Vasily Bulatov and Una Callinan with the use of *mumu* for digitizing video is greatly appreciated. The help with the interferometer and random bits of insight provided by Chris O'Brien are also appreciated.

The importance of the continual support and encouragement by my family is immeasurable. I would finally like to thank all the members of the Sloan Automotive Lab and the PSC for making MIT home.

This work is funded under NASA Microgravity Research Grant NAG3-160 to MIT (contract monitor David L. Urban) and an interagency agreement with NIST (C-32016-C). Additional support was provided by the National Science Foundation through a Graduate Research Fellowship for Brad A. VanDerWege.

BIOGRAPHICAL NOTE

The author attended the University of Michigan—Ann Arbor from September 1990 through May 1994, and received a Bachelor of Science in Mechanical Engineering. He received the J.A. Bursley Prize from the U of M and a Graduate Research Fellowship from the National Science Foundation. He is a member of Tau Beta Pi and SAE, and is an alumnus of the University of Michigan SAE Formula Car Team.

TABLE OF CONTENTS

LIST OF TABLES

LIST OF FIGURES

CHAPTER 1

INTRODUCTION

Halogenated hydrocarbons have been extensively used in fire extinguishing applications. Brominated compounds in particular, such as bromotrifluoromethane, CF_3Br, and bromochlorodifluoromethane, CF_2ClBr (halons 1301 and 1211), have been found to be particularly effective in fire suppression, and have been commonly used in total flooding applications, such as computer rooms, engine bays, aircraft, and even the space shuttle [1,2]. Recent concerns about stratospheric ozone depletion have led to bans on the production of many halogenated hydrocarbons. These bans have affected CFC-related industries; the fire extinguishing industry was particularly hindered because most of the compounds used for fire extinguishing applications have been banned, leaving no clear alternatives. Among the most promising alternatives are fluorinated halocarbons [1,3]. Consequently, a substantial amount of research has been conducted recently to understand the behavior of fluorinated inhibitors in flames.

The effect of halogenated inhibitors on the propagation speed of premixed flames has been studied in both normal gravity and microgravity [4-6]. The addition of the inhibitors is found to substantially decrease the flame propagation speed [5], to the point where microgravity conditions become necessary to keep the flames from being distorted by buoyancy [4]. Addition of inhibitors to the air or fuel of a diffusion flame cause a decrease in the ability of the flame to resist extinction by hydrodynamic forces (i.e. strain rate for extinction of counterflow flames or gas velocity for blow-off of jet or coflow flames) [7-10].

Even though the brominated inhibitors have been used extensively, their action in the flame is not particularly well understood. The bromine atom is thought to separate from the inhibitor molecule early in the reaction [9-12]. The bromine atoms are believed to catalytically recombine highly reactive H and OH radicals into less reactive species such as H_2 and H_2O [9, 13], while the fluorinated inhibitors are believed to capture H radicals to form the stable compound HF. The catalytic nature of bromine action is thought to account for the significant advantage in effectiveness of brominated compounds over fluorine and chlorine compounds [8,10]. Therefore, significantly larger amounts of fluorinated inhibitor are required to cause the same effect on a given flame. In fact, on a mass basis, the addition of fluorinated inhibitors to the

oxidizer is found to be only slightly more effective in extinguishing diffusion flames than addition of nitrogen [8]. Despite this, fluorinated inhibitors retain the advantages of being more effective than diluents on a mole basis and being stored easily as a liquid.

This investigation focuses on the effects of inhibitors on laminar jet diffusion flames, in normal gravity and microgravity. The jet diffusion flame is more complex than a counter-flow diffusion flame in that it is two-dimensional and involves both oxidizer entrainment and diffusion. Flame stability for jet flames is also more representative of fires than counterflow flames. Also counterflow or coflow flames require larger total flows and are therefore more difficult to enclose in a microgravity apparatus. The microgravity environment eliminates buoyant instability and buoyancy-induced flows, thus emphasizing diffusion and momentum-controlled entrainment as mechanisms for inhibitor transport into the flame. A jet flame in a microgravity environment can experience low hydrodynamic strain relative to counterflow or normal-gravity flames. The microgravity flames are typically wider than normal-gravity flames with broadened soot production regions. The inhibitors (CF_3Br, CF_3H) and fuels (CH_4 and CO) used in this investigation are intended to be representative of practical systems, while being simple enough to be amenable to detailed chemical modeling. Since no such investigation of inhibitor addition to microgravity diffusion flames had been previously undertaken, observable effects were unknown. Therefore, the experimental set was exploratory in nature, covering a variety of effects.

CHAPTER 2

PREVIOUS WORK AND BACKGROUND

2.1 HALOGENATED FLAME INHIBITORS

There is a vast body of experimental work on the effects of a variety of halogenated compounds as flame inhibitors in different configurations. Compounds including all four common halogens (fluorine, chlorine, bromine, and iodine) have been tested for their flame inhibiting characteristics. Recent interest has been focused mainly on comparisons between CF_3Br, representing highly-effective brominated compounds, which have been banned due to their ozone-depletion potential, and fluorinated compounds, which are their potential replacements.

The effectiveness of inhibitors has typically been characterized either by the limiting concentration for extinction of diffusion flames or by the decrease in flame propagation speed for premixed flames. Limiting concentrations for extinction of diffusion flames has been measured for a number of different flame systems using a wide variety of inhibitors. These measurements are common and are more realistic regarding fire suppression needs than premixed flames, but the results are often dependent on specific experimental details and are therefore not easily repeatable or transferable to other situations. In one of the earliest investigations, Creitz [7] studied the limiting concentrations of methyl bromide (CH_3Br) and bromotrifluoromethane (CF_3Br) as a function of oxygen concentration for extinction of coflow diffusion flames with a variety of fuels. The results showed that at oxygen concentrations higher than about 25%, CH_3Br became ineffective in extinguishing the flames, while CF_3Br appeared to retain some of its effectiveness to much higher oxygen concentrations. Similarly, at oxygen concentrations above 33%, he showed that CH_3Br will burn as a fuel, demonstrating that it acts partially as a fuel as well as an inhibitor. The effectiveness of CF_3Br compared to diluents was measured by Masri [9] on pilot-stabilized turbulent coflow flames of compressed natural gas (CNG) and liquefied petroleum gas (LPG). He performed experiments to find the limiting concentrations of inhibitor addition to the fuel and air sides of the flame. While the concentration of inhibitor in the fuel required for extinction was much higher than the concentration required in the surrounding air, he estimated that the concentration of inhibitor at the stoichiometric position of the flame at extinction was similar whether it was added from the air or fuel side. Trees *et al.* [10] performed experiments comparing CF_3Br with CF_3H in

methane opposed-jet diffusion flames as a function of strain rate. They showed that it takes roughly four times as much trifluoromethane (CF_3H) as CF_3Br on a mole basis to extinguish a flame at the same strain rate. Eleven different fluorinated and chlorinated inhibitors were compared to CF_3Br in a study by Hamins *et al.* [8]. The counterflow and coflow experiments using liquid fuels with inhibitor added to the air side showed that, on a mass basis, the non-brominated inhibitors all performed similarly to each other and nitrogen, while CF_3Br performed about twice as well. This clearly demonstrates the effectiveness of the bromine atom in flame inhibition.

The effect of inhibitors on laminar flame speeds has been used as a measure of inhibitor effectiveness since flame speeds are a chemical property of the mixture in question and are a useful benchmark for comparison with results of chemical kinetic models. A study of premixed methane and ethane flames inhibited with CH_3Br was performed by Simmons and Wolfhard [11]. They observed that the flame speeds of richer flames were reduced more drastically with inhibitor addition than leaner flames, and they concluded from calculated flame temperatures that the extinction of the flames with inhibitor addition was not due to a decreased flame temperature but rather an increased limit temperature (the minimum flame temperature at which the flame will continue to propagate for a given fuel). Ronney [4] studied premixed hydrocarbon flames inhibited with CF_3Br in normal and microgravity spherical flames, the latter allowing very low flame speeds. He observed that CF_3Br effectiveness decreased at higher pressure, and he noted that methane-air flames could not be ignited above CF_3Br concentrations of about 6%. The reduction in flame speeds of methane-air flames has been studied by Linteris [5] for comparison with numerical results. He also found a decrease in effectiveness per mole of inhibitor at increased concentrations and a greater reduction in flame speeds for rich mixtures.

The mechanism through which halogenated flame inhibitors affect flame chemistry has been investigated with a number of different experimental methods and numerical models. One of the early, key works on the effect of brominated compounds was by Simmons and Wolfhard [12]. They performed spectroscopic studies on flat diffusion flames inhibited with CH_3Br. They showed that when the inhibitor was added to the air, an induced reaction zone was produced on the air side of the flame which emitted frequencies associated with Br_2 chemiluminescence. Therefore, they suggested that this zone is a region of inhibitor decomposition. They also observed a decrease in OH emission and an increase in soot production with the addition of CH_3Br. Ibiricu and Gaydon [14] performed similar spectroscopic measurements using CH_3Br to inhibit methane opposed-jet flames, and found similar results. The appearance of a similar

induced reaction zone is reported by Trees *et al.* [10] for CF_3Br-inhibited methane-air opposed-jet diffusion flames. The appearance of the induced reaction zone with these two different inhibitors, once again suggests that it is produced by the bromine, not the intact inhibitor molecule. Profiles of temperature and concentrations of stable gaseous species were reported by Seshadri and Williams [15] for a counterflow liquid-fuel flame with CF_3Br added to the oxidizer. Their profiles show that the concentration of inhibitor drops off slightly to the air side of the flame, which is consistent with an inhibitor decomposition zone on the air side of the flame. They also noted an increase in soot production with the addition of CF_3Br. Radical concentrations calculated by Masri [9] show a substantial decrease in H, O, and OH radicals but a nearly constant temperature with addition of CF_3Br to the oxidizer. The collective observations for CF_3Br addition to the air side of diffusion flames are an induced inhibitor decomposition zone, decreased concentrations of vital radicals, and increased soot production.

The chemistry through which fluorinated compounds act to inhibit flames has been studied only more recently. Species concentration profiles were measured by Vandooren *et al.* [16] for flames in $CO/H_2/O_2/Ar$ mixtures inhibited by CF_3H at low pressure. They observed a lower conversion of CO to CO_2 resulting in a lower temperature and drastic decreases in H and OH radical concentrations. Hydrogen halide (HF, HCl) production in inhibited propane-air diffusion flames was measured by Linteris [17]. He reported that HF production was up to 25 to 35% below equilibrium levels when the inhibitor was added to the oxidizer, and 45 to 70% below when added to the fuel. He concluded that these results indicate kinetic limitations on the reaction of inhibitors in the flame. Linteris [6,18] also performed extensive numerical modeling of inhibition of $CO/Ar/O_2/H_2$ and methane-air flames with fluorinated methanes. The results include decomposition pathways, which show that reactions of the inhibitor with H and OH radicals are the dominant pathways of inhibitor decomposition in the methane flames, which suggests that the inhibiting effect of fluorinated inhibitors is through reactions of radicals with decomposition products of the inhibitor forming HF (which is relatively stable).

2.2 Microgravity Jet Diffusion Flames

Law and Faeth [2] have thoroughly reviewed the advantages and disadvantages of combustion experiments in microgravity, including effects on nonpremixed flame structure, stability, and soot formation processes.

Experiments on microgravity jet diffusion flames have been carried out primarily by two groups. The work of the first group of Bahadori, Edelman *et al.* has involved a wide range of topics including effects of flow rate, nozzle size, and changes in ambient pressure on flame shape in normal gravity and microgravity, comparisons of flame shape with theory, radiant emission, and transition to turbulence [19-25]. Their measurements show that the ratio of flame height to nozzle diameter is roughly proportional to the jet Reynolds number [19] and that flame height reaches a minimum around a pressure of one atmosphere [20]. Their work on turbulent flames in microgravity shows that the instabilities of transitional flames start from the bottom rather than the top as in normal gravity, and that fully turbulent flames are much taller in microgravity than normal gravity [25]. Their experiments on radiation from jet diffusion flames showed that microgravity flames radiate 6-9 times as much as normal gravity flames and that radiation increases with increasing oxygen concentration.

The second group working on microgravity jet diffusion flames, Faeth *et al.*., has been primarily concerned with soot formation. They performed experiments of laminar smoke point luminosity lengths and soot concentrations using laser extinction on microgravity flames [27], and thermocouple and multiline-emission temperature measurements and thermophoretic sampling on weakly-buoyant (low-pressure, normal gravity) flames [26]. Calculations they performed showed that residence times in the microgravity flames increase with burner diameter and flame length, which justifies their observation that microgravity flames exhibit laminar smoke points [27]. Residence times at laminar smoke points were shown to be an order of magnitude larger for microgravity flames [27]. They also indicate that soot pathlines are drastically different in microgravity [27], and that microgravity flames have larger soot-containing and soot-oxidation regions [28].

The work presented here is the first to combine the fields of inhibition of flames with halogenated compounds and microgravity diffusion flames. While the research has been inspired by chemical inhibition, the results presented here provide insight for both fields.

CHAPTER 3

EXPERIMENTAL SETUP

3.1 APPARATUS

Microgravity conditions were achieved utilizing the 2.2-second drop tower at NASA-Lewis Research Center in Cleveland, OH. The tower has an opening down the center through which the experimental packages fall 23.7 meters. At the top of the tower a winch is used to lift the package up to the release system. At the bottom of the tower, an airbag system is used to decelerate the package. To reduce air drag on the package, it is dropped inside of a drag shield. The drag shield encloses the experimental rig, so that the experimental rig is moving slowly relative to the air around it. This simple system allows for up to 12 drops per day.

The experimental rig used for these experiments was one made available by NASA-Lewis. This rig was designed for gaseous- or solid-fuel combustion experiments. The components of the rig fit into a frame 880 mm high by 960 mm long by 400 mm wide. The flame is contained in a 27 liter (254 mm in diameter ; 533 mm high) sealed chamber (see Fig. 3.1). The pressure of the oxidizing environment was typically measured using the transducer at the gas filling station. The fuel for the flame is injected into the center of the chamber from a 1.7 mm inner diameter stainless-steel tube. The flow rate of the fuel is controlled by a pressure regulator (Brooks Model 8601) and choked-flow orifice (O'Keefe J#SS), and is measured by a mass flow meter (Omega 0-500 sccm FMA-5606-ST). Figure 3.2 shows a schematic of the apparatus. Ignition was achieved using a retractable hot wire (50 mm of 0.25 mm diameter, 30 gauge, KANTHAL A®). The wire is moved into position (across the centerline of the jet about 2 mm above the rim of the tube) using a rotary solenoid (Lucas Ledex H-3084-028). Timing of the fuel flow and ignitor was performed by a programmable electronic controller. The gasses used for these experiments are: methane (American Air Gas, 99.99%), oxygen (NASA stock, 99.5%), nitrogen (NASA stock 99.999%), bromotrifluoromethane (DuPont, 99%), trifluoromethane (Matheson, 99%), and carbon monoxide with 0.01 mole fraction CH_4 (Scott Specialty Gasses, 0.9985% CH_4). Power for the system is provided by three 28-volt rechargeable battery packs.

Optical access to the flame is provided by a 100 mm by 150 mm window on the side of the chamber. LEXAN® was chosen for the window material since the products of the inhibited flames contain HF, which etches glass. Images of the flames are taken with a CCD video

camera (Panasonic WV-CL352) with a 12 mm lens (Panasonic WV-LA1208). The minimum scene illumination for this setup is about one lux. A fiber optic transmitter (Opticomm MM-1090/XMT) sends the video signal to the top of the tower via a fiber optic cable which is attached to the drop package. At the top of the tower, the matching fiber optic receiver relays the signal to a time-code generator and S-VHS VCR.

3.2 PROCEDURE

Between experiments, the batteries were charged, the hot wire was replaced, and the camera gain was set. The camera gain for each experiment was chosen based on an estimate of flame size and luminosity. Because of the different gains for different experiments, the intensity of different images are not directly comparable. Before an experiment, the gasses were introduced and the controller program was loaded. The oxidizing environment of the flame was prepared by evacuating the chamber and adding the components according to their partial pressures in the desired mixture. Components were added in order of increasing mole fraction. For normal pressure experiments, the gasses were mixed, in ratios according to their partial pressures, to a total pressure to 101 kPa. To reduce error in the ratios of components in low pressure experiments, the gasses were also premixed to total pressures of 101 kPa, but then some of the mixture was removed to reach a total pressure of 25 kPa. The fuel storage bottle is then filled to about 500 kPa, and the program is loaded into the controller from a portable computer.

The experimental rig is then loaded into the drop shield, the fiber optic cable is attached, and the package lifted to the top of the tower. At the top of the tower, the program is activated and the VCR is set to record. When activated, the program opens the fuel solenoid for about one-half second to fill the tube with fuel, swings the ignitor arm into position, and then waits for the signal that the drop has begun. Once the package is released, the fuel solenoid is opened, and current is applied to the hot wire. In initial experiments, the current to the hot wire was modulated to keep the wire from overheating, so that it could be reused. After trials with different current schedules, it was determined that the high temperature required to ignite methane quickly and reliably, would not allow the wire to be reused. A simple current schedule of continuous current (which amounts to shorting the wire across one of the 28 volts battery packs) applied for 0.1 seconds was therefore employed. After heating the wire the arm retracts out of the flow field, causing the molten wire to break off the arm, often breaking into many pieces. Flames reached an apparent steady state an average of about one second after ignition, although some flames steadied in as quickly as 0.5 s. and some were still visibly changing at

impact. The fuel flow is stopped about 2.3 seconds after it started, which is shortly after impact. The package is then lifted back up and the experimental rig is removed from the drop shield.

After a series of experiments were complete, the video images of the flames were measured and the visible structure noted. Individual frames of the video were digitized for easy comparison and demonstrative purposes. Digitization was performed using a Silicon Graphics Indigo2 with a Galileo Video system (Model No. CMNB009A). For flames that approached steady state, the frame chosen for digitization was as close to impact as possible. Multiple frames were digitized from experiments that exhibited flame extinction to examine the transient. In these cases, the time code of each digitized frame was noted. Images of low-flow-rate methane flames and of CO flames are presented cropped to a height of 76 mm and images of high-flow-rate methane flames cropped to a height of 113 mm.

3.3 Experiment Set

The set of experiments was designed to explore how chemical inhibition affects the structure of laminar jet diffusion flames in normal gravity and microgravity. Since the nature of the effects of the inhibitor on microgravity flames were not known, a number of parameters were varied to identify any visible effects. The range of conditions tested are shown in Table 3.1. Unless otherwise noted, experimental conditions shown are at the baseline conditions defined as a total pressure of 101 kPa, temperature of 298 ± 4 K, fuel flow rate of 154 sccm (at 15°C), and oxidizer consisting of air (21% O_2 / 79% N_2). Except for cases noted by specific oxygen concentrations, inhibitor addition to the oxidizer mixture implies a corresponding reduction in the air in the mixture, so that addition of a volume fraction, X_i, of inhibitor leads to concentrations of O_2 and N_2 in the oxidizer of $(1-X_i)$ times that of air. See Appendix I for a list of experiments performed.

Table 3.1 Experimental conditions

Fuel	CH_4, CO/CH_4
Nozzle inner diameter	1.7 mm
Fuel flow rate	154 and 308 sccm
Pressure	25 and 101 kPa
O_2 concentration	17.8 - 30%
CF_3Br molar concentration	0 - 3%
CF_3H molar concentration	0 - 15%

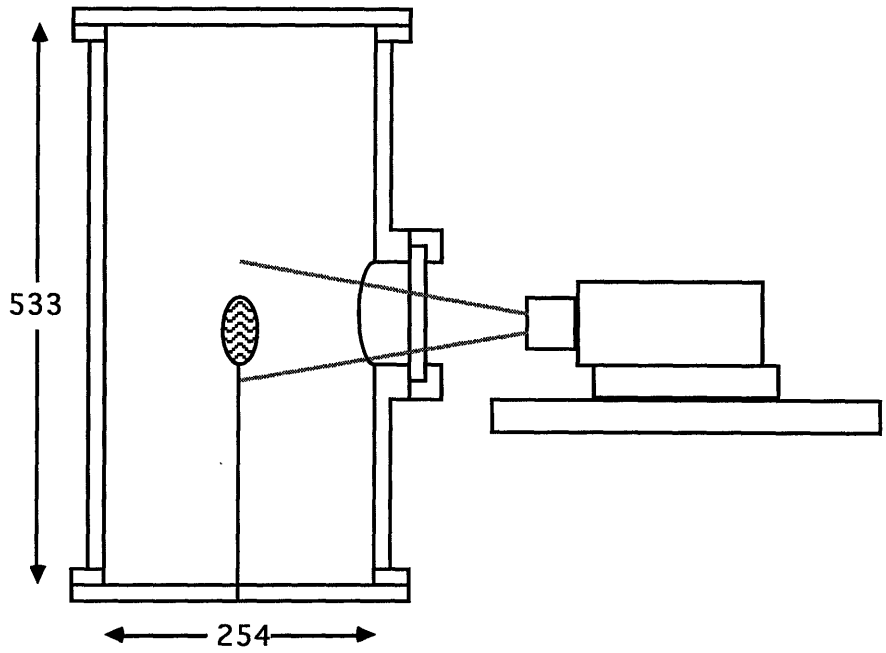

Figure 3.1 Sketch of experiment chamber. Camera views flame through window on side of chamber. Dimensions in millimeters.

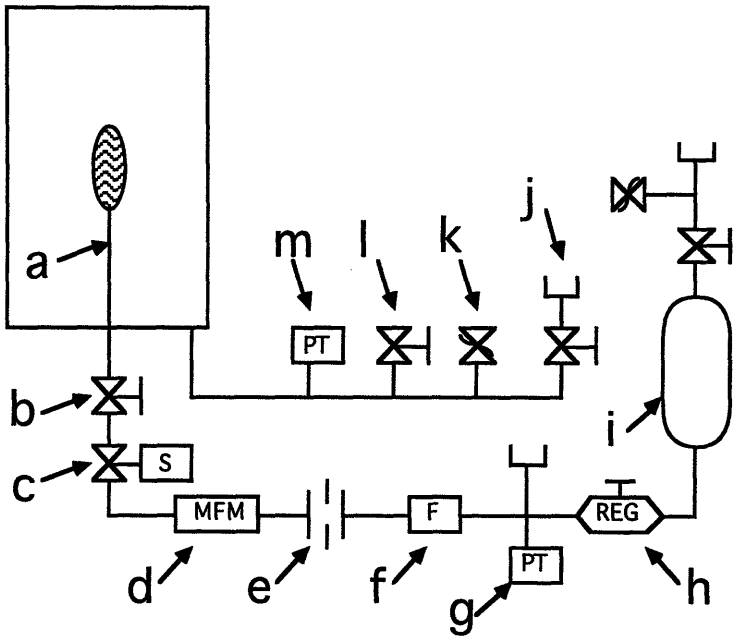

Figure 3.2 Schematic of microgravity apparatus:

a) 1.7 mm ID fuel delivery tube
b) manual valve
c) solenoid valve
d) mass flow meter
e) sapphire flow orifice
f) filter
g) pressure transducer (0-690 kPa)
h) pressure regulator
i) fuel storage bottle
j) quick disconnect
k) relief valve
l) valve for vent
m) pressure transducer (0-345 kPa)

CHAPTER 4

EXPERIMENTAL RESULTS

The experimental conditions for the flames described in this chapter are listed in Appendix I, and images of selected flames are shown in Appendix II. Intensity from one image to another is generally not comparable since the camera gain was varied to increase contrast. The code used to refer to experiments consists of the number of the experimental series, *n* for normal gravity or *u* for microgravity, and the experiment number within the series. Unless noted, percentages of reactants quoted refer to mole fractions.

4.1 Atmospheric Pressure

4.1.1 Normal Gravity

The atmospheric-pressure (101 kPa), normal-gravity flames (1n1-1n6,1n13; Fig. AII.1) provide a reference point for flames subjected to substantial buoyancy. Buoyancy causes instability which is manifested in pronounced flickering. Images of these flames depict a structure with a blue base and sides and a yellow core extending to the pointed tip. The blue luminosity is indicative of the main reaction zone while the yellow inside is soot luminosity. Soot is visible about 5 mm downstream of the rim of the fuel tube at a small distance to the fuel side (inside) of the flame; the blue luminosity of the flame can be seen around the bottom and on the sides of the image. The soot is convected toward the tip, where its luminosity masks that of the flame. Soot distribution of this type is described by Glassman [29] for co-annular flames.

Addition of either CF_3Br or CF_3H to the normal-gravity, 101 kPa flame, up to the point of destabilization, caused no visible change in the flame structure except for increasing the length and flicker amplitude, as indicated in Table 4.1. For 1% CF_3Br (1n4) and 8% CF_3H (1n6), the intense flickering caused packets of flame to break off from the tip. With 1.5% CF_3Br (1n13) in the oxidizer, the flame lifted off the rim of the fuel tube and oscillated 13 to 35 mm above it. At 2% CF_3Br (1n2), the flame lit and immediately blew off. Very similar stability limits for addition of CF_3Br (about 1.7%) were found for natural gas coflow flames by Creitz [7]. Extrapolation of Masri's [9] data for extinction of turbulent coflow natural gas flames with CF_3Br to low-jet-velocity yields a similar stability limit (between 1.5 and 2.5%). Simmons and Wolfhard [12] also indicate that for addition of CH_3Br (which has similar limiting

concentrations to CF_3Br near atmospheric conditions [7]) methane flames cannot be stabilized above a mole fraction of 3.8% in the oxidizer for any fuel flow rate. For CF_3H addition, the stability limit of normal-gravity, 101 kPa flames was found to be around 8%. This value appears to be consistent with published results since stability limits found for both CF_3Br and CF_3H addition resemble those reported for opposed-jet flames at a strain rate of 200 to 250 s^{-1} [10].

4.1.2 Microgravity

4.1.2.1 Uninhibited

An atmospheric-pressure (101 kPa), uninhibited microgravity flame was recorded in each of the three experimental series (1u5, 2u16; Fig. AII.1, 3u1). The flame in the first test (1u5) appears to not be fully developed, and the one in the third test (3u1) shows a substantial side draft, causing asymmetry. The second test (2u16; Fig. AII.1) resembles the preliminary test case (1u1) as well as observations by other investigators [24] and will be adopted as the reference in what follows. The uninhibited microgravity flame (2u16; Fig. AII.1) is 130% wider and 12% longer than the average length of the normal gravity flame, is stable (no flicker), and has a rounded tip. The microgravity flame has a distribution of soot luminosity similar to the normal gravity flame, with the blue main reaction zone visible at the base and around the sides but not at the tip. This flame and the higher-flow-rate flame described in Section 4.1.2.5 (3u5; Fig. AII.7), agree well with the $h/d \approx Re_d/4$ relationship presented by Bahadori and Edelman [21]. This relation is plotted in Figure 4.1 along with experimental data and a model from Bahadori *et al.* [19].

4.1.2.2 CF_3Br Inhibition

Whereas normal-gravity flames show little structural change with the addition of inhibitor, the lack of buoyancy-induced flows in microgravity leads to more pronounced changes in flame structure in the presence of inhibitor. The addition of 1% CF_3Br to the oxidizing environment of the microgravity flame (3u3; Fig. AII.2) produces an open-tipped flame with a pronounced two-zone structure. At the base of the flame, a thin blue region is visible, which is aligned with the interface between the two visible zones. This blue luminosity is presumably the main reaction zone. The inner zone is bright yellow, likely due to soot luminosity, fading to red at the tip. The coloration and flat top of the soot plume suggest that rather than oxidizing while

convecting through the flame front, the soot cools and ceases to emit in the visible range. The combination of the main reaction zone and the inner soot plume resemble the structure of microgravity flames of heavier hydrocarbons, such as propane, which have a blue base and a flat tip fading from yellow to red [19].

The outer zone appears orange, and is about half the height of the soot plume and about 25% wider than the uninhibited flame. A similar structure on the oxidizer side of the flame was observed by Simmons and Wolfhard [12] for flames inhibited by CH_3Br. Their spectrographic analysis shows red and ultraviolet emissions attributed to Br_2 in this zone. They suggest that heat and radicals diffusing from the main reaction zone assist in decomposition of CH_3Br, thus releasing Br. A peak in Br_2 concentration on the oxidizer side of the main reaction zone is also predicted by opposed-jet diffusion flame calculations for CF_3Br addition to the oxidizer [Masri]. The three-part structure (soot, main reaction, inhibitor decomposition) of the CF_3Br-inhibited microgravity flames appears to be analogous to the structure observed in opposed-jet diffusion experiments with CF_3Br added to the oxidizer stream performed at NIST and presented by other investigators [10,15]. At low strain rate, these experiments showed three distinct zones: a thin blue reaction zone in the middle, a bright yellow soot-luminescence zone on the fuel side, and a diffuse reddish zone on the oxidizer side. The reddish color of this oxidizer-side zone is consistent with the red and ultraviolet Br_2 emissions reported by Simmons & Wolfhard [12]. This zone is believed to be a region of CF_3Br decomposition.

In an attempt to reduce the contrast of this flame by reducing soot levels, so that the outer structures could be seen more clearly, an experiment was performed with 1% CF_3Br and reduced oxygen concentration: 18% O_2 / 81% N_2 (2u14; Fig. AII.3). Although this flame was unstable and extinguished, its structure as it extinguished was quite informative. Just 0.30 seconds after ignition, this flame appeared much like the 1% CF_3Br flame in air (3u3; Fig. AII.2), except that it was slightly shorter, did not extend below the rim of the fuel tube, and the soot luminosity was less intense relative to the outer luminous zone, as desired. Over the next 0.13 seconds, the soot luminosity ceased, leaving a nearly cylindrical shell of luminosity which was orange on the outside and appeared to be blue on the inside, which is presumably the inhibitor-decomposition zone and the main reaction zone. The existence of the outer shell without the inner luminous zone is consistent with the presumption that the inner zone is soot luminosity and not a main reaction zone. This flame also demonstrates that the edges of the luminosity of the main reaction zone and the inhibitor-decomposition zone are located adjacently. Support of the inhibitor-decomposition zone thermally and chemically by the main

reaction zone suggests that wherever the main reaction zone ceases to exist, or is too weak to be luminous, it cannot support the inhibitor-decomposition zone. Conversely, this suggests that the main reaction zone in the 1% CF_3Br flame (3u3; Fig. AII.2), may end at the height where the outer luminous zone ends. After soot luminosity has disappeared in the 1% CF_3Br, 18% O_2 flame (2u14), the edges of the flame retreat along the contour of the flame until is has extinguished, 0.67 seconds after ignition.

The experiments conducted with 1.5 and 2% CF_3Br added to the oxidizing environment (1u11, 3u4; Fig. AII.2) demonstrate that increased CF_3Br mole fractions results in a shorter outer luminous zone and a smaller soot plume. At 3% CF_3Br addition (2u13; Fig. AII.2), the flame lit and extinguished. Although the image of this flame was saturated, the flame appeared to extinguish in a fashion similar to the 1% CF_3Br / 18% O_2 flame, retreating along the contour of the flame, except that with this flame, soot luminosity was visible until all luminosity had ceased. The observed stability limit for addition of CF_3Br between 2 and 3% mole fraction is consistent with observations of counterflow methane and liquid fuel experiments [8,10] for strain rates of about 50-100 s^{-1}. As pointed out by Hamins [8] for coflow flames, this supports the contention that these microgravity are stabilized in a region of low stretch.

4.1.2.3 CF_3H Inhibition

The addition of CF_3H to the surroundings of the microgravity flame has a significantly different effect than CF_3Br addition on the structure of the flame. With 1% CF_3H addition (3u12; Fig. AII.4), the flame tip appeared open, and soot luminosity was reduced relative to the main reaction zone compared with the uninhibited flame (2u16; Fig. AII.4). This flame was only slightly shorter and wider than the uninhibited flame (2u16; Fig. AII.4), and did not exhibit a visible inhibitor-decomposition zone. At 2% CF_3H addition (3u10), the flame was nearly identical to the 1% CF_3H flame. The image for the 5% CF_3H-addition experiment (2u9; Fig. AII.4) shows an asymmetry in the flame likely caused by a draft from the side, which may have contributed to the soot luminosity observed. With 6% CF_3H addition (2u6; Fig. AII.4), no soot luminosity was visible. Up through 5% CF_3H (2u9; Fig. AII.4), the length of the flame remained close to the of the uninhibited flame (2u16; Fig. AII.4), and the width had only increased slightly. For 6% CF_3H (2u6; Fig. AII.4), the flame was significantly shorter and wider, so that the downstream ends of the flame no longer converged back towards the centerline of the flame, but were parallel for 6% (2u6; Fig. AII.4) and diverging for 8% CF_3H addition (2u3; Fig. AII.4). This trend continued through 12% CF_3H addition (1u10; Fig.

AII.4), at which point the flame was 22% shorter and 32% wider than the uninhibited flame (2u16; Fig. AII.4). The increase in flame width with CF_3H addition is partially a result of decreased oxygen concentration in the oxidizer mixture, causing the stoichiometric position for the flame to be further out, and increased oxygen requirements of the flame, since CF_3H acts partially as a fuel. The microgravity methane flames with 6-12% CF_3H added to the oxidizer appear to have a shape similar to the main reaction zone in the CF_3Br-inhibited flames (3u3, 2u14; Figs. AII.2,3), which suggests that, despite differences in soot luminosity and inhibitor-decomposition zones, the two inhibitors affect the main reaction zone similarly.

The addition of 15% CF_3H to the oxidizing environment (3u9) caused extinction of the microgravity flame. Like the 6-12% CF_3H flames, this flame lit with a sooty core and the tip opened as the initial soot convected away. But in this case the flame did not stabilize, but continued to retreat along its contour, in a fashion similar to the extinction of the CF_3Br-inhibited flames. As in the case of CF_3Br inhibition, the observed microgravity stability limit for CF_3H addition, between 12 and 15%, is similar to observations of counterflow methane and liquid fuel experiments [8,10] for low strain rates (about 0-100 s^{-1}).

Since flames can be supported with such high concentrations of CF_3H, two experiments were performed to gauge how much of the effect of CF_3H is due to dilution and oxygen concentration reduction. The reference case for this comparison was 8% CF_3H replacing air (19.3% O_2 and 72.7% N_2, 2u3; Fig. AII.5). For the first comparison, 8% CF_3H replaced nitrogen, while the oxygen concentration was kept at 21% mole fraction (71% N_2, 2u4; Fig. AII.5). The replacement of 1.7% O_2 to the oxidizing atmosphere, caused the flame to exhibit an open tip and no soot luminosity; however, the width of the flame decreased by 11% to almost that of the uninhibited flame. Since the comparison case had the same concentration of oxygen in the oxidizer mixture as the uninhibited case but still had an open tip and no soot luminosity, this comparison shows that the reduction in soot luminosity and the opening of the tip are not solely due to the reduction in oxygen concentration caused by CF_3H addition. The 8% CF_3H / 21% O_2 flame remained slightly larger than the uninhibited flame likely due to increased oxygen requirements, since CF_3H acts partially as a fuel. In the second comparison, air was diluted with 8% N_2 rather than CF_3H (19.3% O_2 and 80.7% N_2, 2u5; Fig. AII.5). This flame exhibits soot luminosity and appears to have a closed tip while the flame with the same concentration of CF_3H added to the oxidizer (2u3; Fig. AII.5) had neither. Both of these comparisons (2u4,5; Fig. AII.5) indicate that CF_3H is more effective on a mole basis than nitrogen at reducing soot and causing an open tip.

4.1.2.4 Effect of O_2 Concentration

In order to understand how O_2 concentrations affect soot luminosity and tip opening, two experiments were conducted with nitrogen dilution to the oxidizer. As described above, the flame with 8% N_2 dilution (19.3% O_2 and 80.7% N_2, 2u5; Fig. AII.5), retains some soot luminosity and appears to have a closed tip. The flame with 14.3% N_2 dilution of the oxidizer (18% O_2 and 82% N_2, 3u2; Fig. AII.5), appears similar to the 8% CF_3H flame (2u3; Fig. AII.5) having no soot luminosity, an open tip, and the same width, but about 24% longer. Four experiments were also performed at increased oxygen concentrations. An uninhibited, microgravity flame with 30% O_2 in the oxidizing environment (2u19; Fig. AII.6), was closed-tipped, sooty, and 64% as long and 68% as wide as with 21% O_2. Addition of 3% CF_3Br with 30% O_2 (67% N2, 2u18; Fig. AII.6) did not cause extinction as with the flames in air, but resulted in an open-tipped flame. This flame also exhibited a very dim, very thick outer red luminous zone, consistent with zones observed on other CF_3Br-inhibited flames, which is presumed to be a region of inhibitor decomposition. Addition of 8 and 12% CF_3H with 30% O_2 (62% N_2, 58% N_2; 2u10,12; Fig. AII.6) caused the flame to become larger, as expected by the change in stoichiometry, but soot luminosity and the closed tip persisted in contrast to the flames in 21% O_2. These experiments show that at higher oxygen concentrations microgravity flames are more likely to produce soot and are more resistant to extinction by addition of inhibitors, as expected from normal gravity experiments [7,29]. A more interesting result is that flame tip opening appears to require less inhibitor at lower oxygen concentrations, to the point where no inhibitor is required, around 18% O_2.

4.1.2.5 Effect of Higher Flow Rate

A subset of the methane experiments were also performed with a fuel flow rate of 308 sccm, which is twice that of the baseline case. Adjusting the camera gain for these flames proved to be difficult, since they occupied a much larger portion of the field of view so the camera adjusted to them differently. The higher-flow-rate flames were also more susceptible to asymmetry caused by side drafts, which were possibly caused by the rotation of the ignitor arm. The camera gain for the high-flow-rate, uninhibited flame (3u5; Fig. AII.7) was too low, so only the soot luminosity can be seen. The height of this flame was estimated from the curvature of the soot luminosity. The estimated height is about twice that of the low-flow-rate flame, which agrees with data from other investigators (Fig. 4.1), and the width of this flame is roughly the same as

that of the low-flow-rate, uninhibited flame. The tip of the luminous soot for this flame does not look obviously open or closed. The following experiment, with 1% CF_3Br added to the oxidizing environment of the high-flow-rate flame (3u6; Fig. AII.7) also suffered from too low camera gain. This flame appears shorter than the uninhibited flame and the curved shape of the tip suggests that it is closed-tipped. The observation that the 1% CF_3Br flame appeared closed-tipped at the higher flow rate (3u6; Fig. AII.7) and open-tipped at the lower flow rate (3u3; Fig. AII.2), suggests that the flame is more susceptible to tip opening at lower flow rates. This is consistent with observations by Bahadori *et al.* [19] that it is possible to obtain open-tipped uninhibited microgravity methane flames at lower flow rates than used here. Since the low-flow-rate experiments suggest that inhibitor addition increases tendency for tip opening, the apparent closed tip of the 1% CF_3Br flame implies that the uninhibited flame should be closed-tipped. The camera gain for the experiment with 2% CF_3Br in the oxidizing environment (3u7; Fig. AII.7) was too high to obtain sufficient contrast, so that the interior of the flame is saturated and only its outline can be seen. However, this flame appears to have a two-luminous-zone structure similar to the corresponding low-flow-rate case, although it is significantly longer.

For 8% CF_3H addition to the oxidizing environment at high-flow-rate (3u8; Fig. AII.7), a sooty and very tall (>100 mm) flame was observed. Since the tip of the flame went out of the viewing range of the camera, it is impossible to tell if it was open tipped or not. The fact that this flame was sooty while the low-flow-rate flame under the same conditions (2u3; Fig. AII.4) was not indicates that the higher-flow-rate flames have a higher propensity for soot production. In contrast to the low-flow-rate flame, the high-flow-rate flame with 15% CF_3H addition did not extinguish, but was open-tipped and showed no soot luminosity. This set of experiments indicate that at higher flow rate these microgravity methane flames are more likely to have soot luminosity and a closed tip, and are more resistant to inhibitor-induced extinction, which is in direct contrast to normal-gravity flames.

4.2 Low Pressure

Low-pressure, normal-gravity experiments have been used to simulate the low-buoyancy conditions of microgravity and allow experimental study to complement microgravity experiments. Since buoyant force scales as p^2g [2], buoyant effects should be small at low pressure. Thus, in principle, low pressure flames should behave similarly to flames in microgravity. Clearly, other effects also scale with pressure (e.g. diffusion and reaction rates),

which may offset the dynamic similarity. The 25 kPa flames tested here should experience only 6% of the buoyancy of the 101 kPa flames. The usefulness of such low-pressure experiments depends on how low the pressure needs to be for buoyancy to be negligible, and whether the behavior of flames at such low pressures is analogous to behavior at common pressures.

4.2.1 Normal Gravity

The uninhibited, normal-gravity, low-pressure (25 kPa) flame recorded (1n10; Fig. AII.1) was twice as wide and 12% shorter than the atmospheric-pressure flame (1n1; Fig. AII.1). This flame was also non-flickering, oval in shape, and exhibited no soot luminosity. The lack of flickering and the change in shape are likely due to the reduction of buoyancy-induced flow instability. Buoyancy draws the hot gasses inward and upward causing the flame to be taller and thinner [27]. The decrease in soot levels for the low-pressure flames is usually attributed to a combination of a decrease in absolute soot-precursor concentrations [29] and a decrease in residence time [27]. This flame and all the low-pressure flames tested (including the one at 30% O_2) showed a diffuse halo of luminous gasses around the main reaction zone. In all but the CF_3Br-inhibited flames, the halo was a pale blue color, consistent with emissions from CO oxidation. Since CO oxidation occurs on the oxidizer side of the flame and involves relatively slow chemistry which may be slowed further by the decrease in pressure, it seems reasonable that the halo is a region of reaction involving CO oxidation. For this flame, the halo was blue and thicker on top than on the sides, possibly due to broadening of the zone by increased flow velocity at the tip, caused by buoyant flow. Addition of 1% CF_3Br to the oxidizer environment of this flame (1n12; Fig. AII.8), caused the flame to lift off the rim of the fuel tube by 25 to 35 mm. The fact that the 101 kPa flame did not lift off at concentrations up to 1.5% CF_3Br, indicates that the 25 kPa flame is slightly less resistant than the 101 kPa flame to destabilization by inhibitors. The CF_3Br addition also caused the formation of a diffuse reddish tail on the outside of the blue halo. The coloration of this tail is consistent with emission from Br_2 from the decomposition of the inhibitor, as described in Section 4.1.2.2. At 2% CF_3Br addition (1n14), the flame quickly blew off when the ignitor was removed. Addition of 4% CF_3H to the oxidizer environment of the normal-gravity, 25 kPa flame [4n1; Fig. AII.8] caused a slight increase in the height and width of the flame. At 5% CF_3H addition the flame extinguished, which is less than the 8% to which the 101 kPa flame survived.

4.2.2 Microgravity

The uninhibited, microgravity, low-pressure (25 kPa) flame (2u2; Fig. AII.9) was 9% longer and 25% wider than the normal-gravity, low-pressure flame (1n10; Fig. AII.8), but is 22% shorter and 9% thinner than the 101 kPa, microgravity flame (2u16; Fig. AII.1). This flame was closed-tipped with no soot luminosity, and it had a broad blue halo which was nearly the same thickness on the sides as at the tip. Addition of 1% CF_3Br to the oxidizing environment of the low-pressure, microgravity flame (1u12; Fig. AII.9) caused a 51% increase in length and 25% increase in width, but the flame tip was still closed. In fact, none of the low-pressure flames observed demonstrated tip opening. This may be due to decreased residence times for low-pressure flames. An increase in size with the addition of inhibitor to the oxidizer is expected because of the decrease in oxygen concentration, but the large jump in size from the uninhibited case to the lower concentration of each inhibitor suggests that the uninhibited case may have been abnormally small. The 1% CF_3Br flame (1u12; Fig. AII.9) also exhibits a reddish halo, similar to the tail observed on the corresponding normal-gravity flame (1n12; Fig. AII.8), but in this case there is no diffuse blue region between the reddish region and the main reaction zone. The halos of the CF_3Br-inhibited flames appear broader than the halo of the uninhibited flame, which may be due to decreased OH radical concentration resulting in a broadened region of CO oxidation or may simply be due to increased luminosity causing the halo to be visible further out. Soot luminosity is visible in the upper half of this flame, while there was none in the uninhibited flame (2u2; Fig. AII.9). An increase in soot production with the addition of brominated inhibitors or bromine itself has been reported by a number of investigators [12,14,15,29]. Also, the main reaction zone of the 1% CF_3Br, low-pressure, microgravity flame appears green in color, which has been noted by a number of investigators for addition of brominated inhibitors, and has been attributed to increased C_2 emissions [9,10,12,15]. Increasing the concentration of CF_3Br in the oxidizing environment to 2% mole fraction (1u13; Fig. AII.9), resulted in a flame which is 71% longer and 30% wider than the uninhibited flame (2u2; Fig. AII.9) with more of its area exhibiting soot luminosity than the 1% CF_3Br flame (1u12; Fig. AII.9). The tip of this flame remains closed, but unlike any other microgravity flame it appears pointed. The halo of this flame was brighter than that of the 1% CF_3Br flame and more yellow in color. Also this flame curved outward at the base, as did the lifted flames (1n12; Fig. AII.8, 1n13), indicating that this flame may have been on the verge of instability. Two attempts were made to ignite the flame at 3% CF_3Br addition [2u17], but neither was successful. Therefore the stability limit with addition of CF_3Br for this flame is

presumed to be between 2 and 3% mole fraction, which is similar to that for the 101 kPa, microgravity flames.

Addition of 4% CF_3H to the oxidizing environment of the low-pressure, microgravity flame (2u7; Fig. AII.9) caused a 34% increase in length and a 20% increase in width. This flame was closed-tipped with a blue halo and no soot luminosity. Addition of 8% CF_3H (2u8; Fig. AII.9) produced a flame which appears similar to that with 4% CF_3H (2u7; Fig. AII.9), but it is 51% longer and 30% wider than the uninhibited flame. The stability limit of the low-pressure, microgravity flame with CF_3H addition was not found, but is shown to be over 8% mole fraction.

4.3 CO / CH_4 Fuel

A subset of experiments were performed with carbon monoxide (CO) fuel to observe the effect of the inhibitors on a non-sooting fuel. In order to increase the rate of the CO chemistry, and therefore make the flames more stable, a source of hydrogen was needed to allow for OH radical formation. The fuel available contained 1% mole fraction methane for this purpose. The difficulty that arose in using this fuel was that the flames were very small for the fuel tube and flow rates used for CH_4, since CO only requires one atom of oxygen per fuel molecule rather than four for CH_4. This significantly smaller demand for oxygen causes the stoichiometric position to be much closer to the fuel jet for the CO flame than for the CH_4 flame, resulting in a smaller flame. The smaller CO flame only occupied a small portion of the camera's field of view, and, therefore, had poor resolution. In order to enlarge the flames, keeping the optical setup unchanged, experiments were initially performed at the higher flow rate (308 sccm). The high-flow-rate, uninhibited, microgravity, CO flame (3u14; Fig. AII.10) was blue and closed-tipped. The reaction zone of this flame appeared to be thicker than that of methane, which is consistent with the slower chemistry. The addition of 2% CF_3H to the oxidizing environment (3u16; Fig. AII.10) produced a flame which was slightly larger than the uninhibited one. The addition of 3% CF_3H (3u18) or 0.5% CF_3Br (3u21) caused the flame to blow off immediately after the ignitor was removed. Above 3% CF_3H (3u15,17), the flame would not ignite. The mode of extinction in this case was drastically different from the microgravity methane flames which, rather than blowing off, extinguished without the reaction zone convecting downstream. The blow-off mode of extinction indicates that the flame is destabilized by the velocity of the jet and the flame would, therefore, likely be more stable at a lower fuel flow rate. Because of this contention, low-flow-rate CO flames were also produced to allow higher concentrations of

inhibitor before extinction. The uninhibited, microgravity flame at the lower flow rate (154 sccm; 3u24; Fig. AII.10) was shorter and slightly wider than the high-flow-rate flame (3u14; Fig. AII.10). At this flow rate, the flame was stable with 0.5% CF_3Br addition (2u23; Fig. AII.10), while the high-flow-rate flame was not, which is opposite the trend with flow rate suggested above for CH_4. This inhibited flame was only slightly larger than the uninhibited flame (3u24; Fig. AII.10) and it remained blue and closed-tipped. In the CO flames, no outer red/orange luminous zone was seen as with the CF_3Br-inhibited methane flames, possibly due to the low concentration of inhibitor used and the low camera gain resulting from the highly luminous CO flames.

Table 4.1 Normal gravity flame heights

Inhibition	average ± flicker *(mm)*
Uninhibited	40±10
1% CF_3Br	57±25
4% CF_3H	45±12
8% CF_3H	50±15

(101 kPa, 154 sccm CH_4)

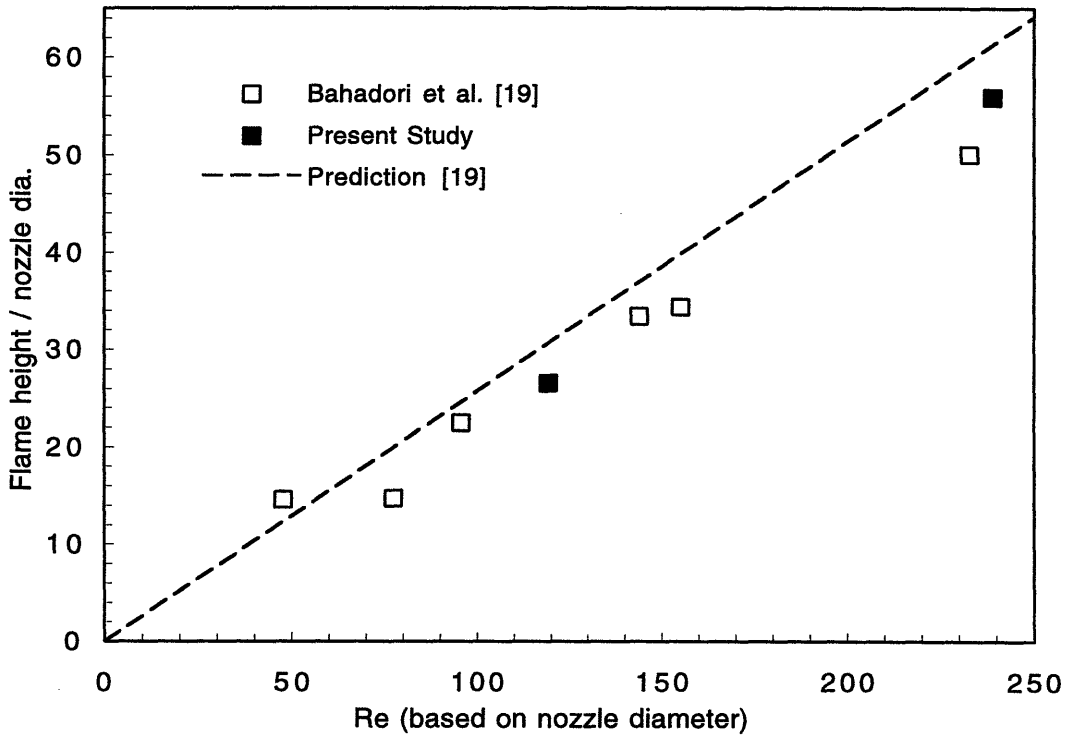

Figure 4.1 Nondimensionalized flame height versus Reynolds number for uninhibited microgravity jet diffusion flames in air. Pressure = 101 kPa. Open symbols and prediction form Bahadori *et al.* [19].

CHAPTER 5

ANALYSIS AND SUMMARY

5.1 STABILITY

The stability limits for the addition of CF_3Br and CF_3H to the oxidizing environment of the methane and carbon monoxide flames found in this work are shown in Table 5.1. These stability limits demonstrate that CF_3H is only about one quarter as effective on a volume basis and half as effective on a mass basis as CF_3Br at extinguishing flames when added to the oxidizing environment. This result is consistent with observations by Trees et al. [10] for methane-air opposed jet flames inhibited with CF_3Br and CF_3H. Hamins et al. [8] also showed that a number of fluorine- and chlorine-based inhibitors had roughly the same limiting mass fraction when added to the oxidizer of a coflow, liquid-fuel diffusion flame. Their reported ratio for the limiting mass fractions for fluorine- and chlorine-based-inhibitor addition to CF_3Br addition is also about 2:1 on a mole basis. Second, most cases exhibit fairly similar limit concentrations for low and atmospheric pressure, except for CF_3H at normal gravity which indicates that the low pressure flames are less resistant to extinction. Third, the normal gravity flames have consistently lower limiting concentrations of inhibitors than the microgravity flames, indicating that even the 25 kPa, normal-gravity flames are destabilized by their buoyancy and are therefore not representative of microgravity flames at least in terms of stability limits. Fourth, the experiments indicate that the limiting concentration is higher at the higher fuel flow rate, which is in contrast to trends in normal gravity and observed results for the CO flames (as described below). Fifth, as expected, the flames appear more resistant to extinction by inhibitor addition at higher oxygen concentrations, in agreement with observations for normal-gravity flames [7].

The final interesting point to note about the stability limits given in Table 5.1, is that the two fuels, CH_4 and CO, have opposite sensitivity of stability limits to fuel flow rate in microgravity. The methane flame appears to be more resistant to extinction at the higher flow rate while the carbon monoxide flame appears to be less resistant. This trend seems consistent with the manner in which the flames of each fuel extinguished. The carbon monoxide flames blew off, which indicates that the limiting factor in their extinction was their ability to remain attached to the rim of the fuel tube. This flame, like a normal-gravity flame, should therefore be destabilized by an increase in the fuel jet velocity. The contour of the methane flames while

extinguishing, on the other hand, remained essentially fixed in position relative to the fuel tube while the flame retreated along the contour from upstream and downstream simultaneously (see images of 2u14; Fig. AII.3). This very different manner of extinction does not appear to be due to destabilization by the jet velocity. The time it takes for the methane flames to extinguish is on the order of the time for the non-extinguishing flames to develop, which suggests that the extinction may be the response of the weakened flame to the accumulation of products in the flame region. This theory is consistent with the observation that the flame is more resistant to extinction at the higher flow rate, since the higher flow rate should lead to entrainment of more fresh oxidizer. This is further supported by the observation that low coflow velocities are sufficient to sustain combustion in microgravity flames which would otherwise extinguish [19]. These two modes of extinction suggest that a given flame may be destabilized in microgravity by too low a flow rate and too high a flow rate. That the normal-gravity flames extinguish through blow-off makes sense in this context, since the buoyancy-induced flows in normal gravity very effectively remove products and increase gas flow velocities, destabilizing the attachment of the flame at the rim. The difference in behavior between the two fuels may be partly due to the fact that, since the CO flame is smaller (closer to the centerline of the jet), it resides in a region of higher gas velocities, although differences in chemistry will certainly play a role.

The inhibition by bromine containing compounds is generally believed to be caused by the bromine atom itself in reactions such as the following sequence [13,29]:

$$Br + RH \rightarrow R + HBr \quad (5.1)$$

$$H + HBr \rightarrow H_2 + Br \quad (5.2)$$

$$OH + HBr \rightarrow H_2O + Br \quad (5.3)$$

Through these reactions H and OH radicals are catalytically recombined into less reactive species H2 and H2O. Since fluorine-based inhibitors are much less effective and HF is so stable, it seems unlikely that fluorine reacts in a similar way. Calculations also indicate that moderate concentrations of Br and Br_2 should be found in inhibited flames [9], but very little free fluorine should exist [18,30]. Part of the effect of addition of fluorinated compounds may be due to reduction in the flame temperature (thermal dilution). However, the mass specific heat of CF_3H is 30% lower than that of N_2, while experiments suggest that they have roughly equivalent limiting mass fractions for extinction [8]. Equilibrium calculations for stoichiometric

mixtures of oxidizer and fuel, as described in Appendix III, show that the equilibrium temperature is nearly the same for equal mole fraction additions of N_2 or CF_3H (since CF_3H releases energy upon reaction; Table AIII.2). This indicates that, since CF_3H is more effective on a mole basis at inhibiting the flame, inhibition by CF_3H must be at least partially due to a chemical effect. The obvious chemical effect for fluorinated compounds is the formation of HF which calculations indicate typically consumes H and OH radicals [5,30]. If this is the main effect of fluorine-based inhibitors, the effectiveness of these inhibitors on a mole basis may be roughly proportional to the number of fluorine atoms they carry. This is consistent with the observation that fluorinated inhibitors have a similar effect on a mass basis [8], assuming that the number of fluorine atoms in the inhibitor molecule is roughly proportional to its mass.

An interesting point to note from the stoichiometric, adiabatic equilibrium calculations for CF_3H addition shown in Appendix III is that the temperature falls by about 10 K per mole percent inhibitor, up to the point where the number of F atoms in the system equals the number of H atoms. Beyond this point the calculated temperature falls much more quickly. Product concentrations from these calculations show that when the number of F atoms is higher than the number of H atoms, nearly all of the hydrogen is used to form HF, thus preventing the heat release that usually results from H_2O formation and resulting in a much lower temperature. The corresponding mole fraction of CF_3H in the oxidizer, for $n_H = n_F$ for stoichiometric methane reaction is 12.3%. That is within the range of limiting concentrations for the 101 kPa, microgravity methane flame, although the diffusion correction discussed in Appendix IV suggests that concentrations at the flame will not exceed 9.3% before extinction. The low concentration of hydrogen in the CO fuel led to the condition of $n_H = n_F$ at a mole fraction of CF_3H of 0.8%, but the flame survived up to 2% CF_3H addition. A similar condition for CF_3Br (concentration of halogen atoms equals hydrogen atoms) would lead to a mole fraction of 9.5% for methane, which is a factor of 3 higher than required. Since bromine acts as a catalyst, much less is required to have a similar effect on the H atom population.

5.2 Soot Production

Soot production in the flames in the experiments described here, as interpreted by visible yellow luminosity, is one of the most easily observable changes in the flame structure. The distribution of soot in the observed flames is consistent with the description given by Glassman [29] for co-annular flames. Soot luminosity begins about 5 mm up from the base of the flame and is concentrated in an annular region 2-3 mm inside the main reaction zone.

Throughout these experiments, soot luminosity was found to increase with CF_3Br addition, increased fuel flow rate, and increased oxygen concentration, and to decrease with CF_3H addition. The increase in soot levels with increased oxygen concentration is explained by the increase in the flame temperature which in turn leads to increased soot production [29,31]. The increase in soot levels with increased fuel flow rate is likely due to an increase in fuel residence time with increasing flame length [27], which increases time for soot pyrolysis kinetics [29].

The increase in soot production with the addition of brominated inhibitors or bromine itself has been reported by a number of investigators [12,14,15,29]. Brominated inhibitors are believed to decompose, releasing the bromine atom, which acts through Eq. 5.1 to dehydrogenate fuel molecules [29]. The resulting unsaturated hydrocarbon molecules combine to form soot [13].

The mechanism through which CF_3H decreases soot production is not as well understood. Fluorine atoms should be very effective at dehydrogenating fuel molecules to increase soot production, as does bromine, but the decrease in soot luminosity with the addition of CF_3H indicates that this does not occur at significant levels. The catalytic cycle suggested for bromine inhibition creates free bromine which can attack the fuel molecule, but the high stability of HF may not allow for significant amounts of free fluorine. Indirect effects, such as flame temperature and radical concentrations, may, therefore, be responsible for the decrease in soot production with CF_3H addition. As described in Section 4.1.2.3, experiments with 8% CF_3H, 8% CF_3H / 21% O_2, and 8% N_2 (2u3,4,5; Fig. AII.5) show that CF_3H is more effective at reducing soot luminosity than N_2 on a mole basis. The higher molar specific heat of CF_3H would seem to explain this, but the heat release from the reaction of CF_3H offsets its heat capacity to some extent. In fact, the stoichiometric equilibrium calculations, shown in Appendix III (Table AIII.2), show nearly identical temperatures for 8% N_2 addition and 8% CF_3H addition (2144 and 2146 K). The corresponding values for the uninhibited case and 8% CF_3H / 21% O_2 are also very similar (2130 and 2126 K), indicating that CF_3H has the same effect on equilibrium temperature as N_2, at low concentrations. If the lower diffusion rate of CF_3H towards the flame (relative to N_2) is taken into account, the amount of inhibitor reaching the flame is lower than in the far field, as shown in Appendix IV, which gives a higher flame temperature for 8% CF_3H than 8% N_2 (2178 versus 2144 K), neglecting non-equilibrium effects. A higher flame temperature for CF_3H addition is contradictory to the observation that it is more effective at reducing soot levels than N_2. These results indicate that the reduction in soot by CF_3H appears to be due to a chemical effect. Glassman [29] indicates that the

availability of H radicals is important in fuel pyrolysis. Calculations show that CF_3H addition reduces H radical concentrations beyond that caused by thermal effects [5]. Therefore, it may also reduce soot production beyond a nitrogen-diluted flame of the same temperature.

5.3 Tip Opening

A number of the 101 kPa, microgravity flames exhibited no indications of a distinct flame zone at the tip when fully developed. The soot of CF_3Br-inhibited flames was convected downstream and did not appear to oxidize, but rather cool as it moved away from the flame, in a manner similar to microgravity flames of heavier hydrocarbons [19]. As the CF_3H-inhibited flames developed, the initial sooty core, found in most flames, convected through the flame tip and no luminosity was observed in the tip region afterwards. Although it is possible that there is a flame zone at the tip of these flames which cannot be detected by the camera, it seems unlikely that such a drastic reduction in luminosity could exist within a hydrocarbon diffusion flame without local extinction. Tip opening has been described by Bahadori *et al.* [19] for microgravity methane flames at Reynolds numbers under 100 (based on jet diameter) filmed at a rate of 15 frames/sec. Propane flames are also shown to transition from open-tipped to closed-tipped at a Reynolds number of about 2000 [21], although this is also the range in which they experience a transition to turbulent flames, so the change may be due to different effects.

The experiments presented here indicate that the tendency for tip opening is increased with decreased oxygen concentration, decreased fuel flow rate, and addition of inhibitors. These trends are the same as for extinction, which suggests that the mechanism that leads to tip opening may be related. Considering that tip opening appears to be a partial extinguishing of the flame tip at a lower inhibitor concentration than required for extinction, tip opening is a precursor to extinction in the manner exhibited by microgravity methane flames (i.e. not blow off). In Section 5.1, product accumulation was suggested as the mechanism causing the extinction of the microgravity methane flames. Similarly, product accumulation at the tip of the flame may be the cause of the observed tip opening. Product concentrations should be highest near the tip of the flame, so the tip should be the first part of the flame to respond to product accumulation. At higher flow rates, the increased momentum should aid removal of products, which are produced at roughly the same rate per unit flame area as at the lower flow rate. The experiments showed that, as the flame is weakened by nitrogen dilution, tip opening occurs. The same effect should be true for inhibited flames, but less inhibitor than nitrogen is required to weaken the flame to the same extent. Flames inhibited by CF_3Br may have an additional

effect. Since bromine acts catalytically, the products of a CF_3Br-inhibited flame (HBr, Br_2) can still effectively act as an inhibitor. So if the products of the lower part of the flame are carried towards the tip, bromine is approaching the flame from both sides, and may achieve higher concentrations than experienced at the bottom of the flame.

An effect similar to tip opening was observed at the base of the flame near extinction—the flame pulls away from the fuel tube at the base of the flame. This may be the response of the weakened flame to the higher velocities near the fuel jet or heat loss to the fuel tube.

5.4 SUMMARY

The effects of CF_3Br and CF_3H addition to the oxidizing environment of laminar jet diffusion flames in normal gravity and microgravity have been studied. A number of experiments were performed using methane as fuel and a few using carbon monoxide. Inhibitor concentrations were varied for different cases of fuel flow rate, oxygen concentration in the oxidizer, and ambient pressure. The following conclusions were drawn from studying video images of the flames and comparing our observations with equilibrium calculations and published observations for similar systems.

1. Addition of CF_3Br to the oxidizer at atmospheric pressure in microgravity produces a flame with two luminous zones. The main reaction zone appears to exist at the boundary of the two luminous zones with soot luminosity as the inner zone and the outer zone is presumed to be a region of inhibitor decomposition. The green color of the low-pressure, CF_3Br-inhibited flames is consistent with observations that CF_3Br addition increases C_2 emissions. Low-pressure experiments also confirm that CF_3Br addition increases the propensity for soot production. Addition of CF_3H to the atmospheric-pressure, microgravity flame decreases soot levels, and at high enough concentrations causes the flame to appear to have an open tip. No separate decomposition zone is observable for CF_3H.
2. The limiting concentration of inhibitor in the oxidizer for methane flame stabilization is about twice as high in microgravity as in normal gravity at atmospheric pressure (101 kPa; about 3% versus 1.5% for CF_3Br and about 8% versus 15% for CF_3H). Limiting concentrations for extinction indicate that CF_3Br is about twice as effective on a mass basis and about four times as effective on a mole basis as CF_3H. The experiments suggest that the resistance to extinction by addition of inhibitors of the microgravity methane jet diffusion flames is increased with increasing oxygen concentration, and is not a strong function of ambient

pressure. The resistance to extinction is also increased with increasing flow rate in this range, contrary to results with normal-gravity flames. At low pressure (25 kPa) the stability limits are more similar between normal gravity and microgravity, but results indicate that the limiting concentration of inhibitor is still higher in microgravity. This suggests that normal-gravity flames at 25 kPa are not representative of microgravity flames, at least in terms of extinction.

3. Propensity for soot production in microgravity appears to increase with increasing oxygen concentration, increasing fuel flow rate, and CF_3Br addition, and appears to decrease with CF_3H addition. Stoichiometric equilibrium calculations indicate that inhibition and reductions in soot luminosity by CF_3H addition are likely chemical as well as thermal in nature.
4. The tendency for flame tip opening to occur in the microgravity methane jet diffusion flames is increased with decreasing oxygen concentrations, decreasing fuel flow rates, and the addition of halogenated inhibitors. These trends are the same as for extinction limits for microgravity methane flames, indicating that the mechanisms leading to each might be related. Product accumulation is a possible candidate to explain flame tip opening.
5. The microgravity carbon monoxide flames are significantly smaller than methane flames and exhibit thicker reaction zones and no soot luminosity. The only observable change in these flames with inhibitor addition was an increase in size. Extinction of the CO flames occurred at significantly lower inhibitor concentrations than for methane flames (0.5% versus 3% for CF_3Br and 3% versus 15% for CF_3H). The mode of extinction for the CO flames was drastically different from the microgravity CH_4 flames. The CO flames blew off in a fashion similar to normal-gravity flames, while CH_4 flames extinguished without the reaction zone convecting downstream. These extinction transients suggests that CO flames may be destabilized by the jet velocity, while CH_4 flames may be destabilized by product accumulation.

As these conclusions show, this study provides insight into the effects of CF_3Br and CF_3H on laminar jet diffusion flames of CH_4 and CO in normal gravity and microgravity. The data from the experiments are in terms of extinction limits and images of the flames, from which conclusions have been drawn about the effectiveness of the inhibitors, the mechanism through which the inhibitors act, and the structure and dynamics of the microgravity diffusion flame. These conclusions provide insight into selection of inhibitors for replacement of CF_3Br and guidance for future work.

In order to gain a better understanding of the structure of chemically inhibited diffusion flames and, therefore, the mechanism through which inhibitors act, future work will need to focus on additional diagnostics to give quantitative results such as temperature profiles and species concentrations. The limited time, space, and power available with microgravity experiments will limit many such diagnostics to use in normal gravity. An interferometric method of measuring the temperature field of the flame is being considered for use in drop tower experiments, while gas sampling is an attractive option to obtain species concentrations in normal gravity flames. Thermocouples can also be used in normal gravity to calibrate the interferometry system. To achieve long-term steady-state conditions for the normal gravity flame, a coflow system is planned to supply the flame with fresh oxidizer. Optical absorption methods could also be employed either in normal or microgravity to obtain species or radical profiles in the flame. Chemical kinetic modeling of the inhibited diffusion flame is also planned.

Table 5.1 Stability Limits

Fuel	g	Fuel flow (sccm)	Oxidizer	Pressure (kPa)	Limiting Fraction Mole (%)	Limiting Fraction Mass (%)
CF_3Br						
CH_4	ng	154	air	101	1.5 to 2	7.3 to 9.5
CH_4	ng	154	air	25	1 to 2	5.0 to 9.5
CH_4	µg	154	air	101	2 to 3	9.5 to 13.8
CH_4	µg	154	air	25	2 to 3	9.5 to 13.8
CH_4	µg	154	30% O_2	101	> 3	> 13.8
CH_4	µg	308	air	101	> 2	> 9.5
CO	µg	308	air	101	< 0.5	< 2.5
CO	µg	154	air	101	> 0.5	> 2.5
CF_3H						
CH_4	ng	154	air	101	about 8	about 17.4
CH_4	ng	154	air	25	about 5	about 11.3
CH_4	µg	154	air	101	12 to 15	24.9 to 30
CH_4	µg	154	air	25	> 8	> 17.4
CH_4	µg	154	30% O_2	101	> 12	> 24.9
CH_4	µg	308	air	101	> 15	> 30
CO	µg	308	air	101	2 to 3	4.7 to 7
CO	µg	154	air	101	unknown	unknown

REFERENCES

1. Pitts, W.M., Nyden, M.R., Gann, R.G., Mallard, W.G., and Tsang, W. "Construction of an Exploratory List of Chemicals to Initiate the Search for Halon Alternatives." NIST Technical Note 1279 (1990).
2. Law, C.K. and Faeth, G.M. "Opportunities and Challenges of Combustion in Microgravity." *Prog.Combust. Sci.* **20**, pp 65-113 (1994).
3. Grosshandler, W.L., Gann, R.G., Pitts, W.M., Eds. "Evaluation of Alternative In-Flight Fire Suppressants for Full-Scale Testing in Simulated Aircraft Engine Nacelles and Dry Bays." National Institute of Standard and Technology, Gaithersburg, MD; NIST SP 861, pp 467-641 (1994).
4. Ronney, P.D. "Effect of Gravity on Halocarbon Flame Retardent Effectiveness." *Acta Astronautica* **12** (11), pp 915-921 (1985).
5. Linteris, G.T. and Truett, L.F. "Inhibition of Premixed Methane-Air Flames by Fluoromethanes," accepted for publication in Combustion and Flame, June 1995.
6. Linteris, G.T., "Effect of inhibitor concentration on the inhibition mechanism of fluoromethanes in premixed methane-air flames," Halon Replacements: Technology and Science, American Chemical Society Symposium Series (A.W. Miziolek, and W. Tsang, Eds.), Washington D.C., 1995, pp. 260-274.
7. Creitz, E.C. "Inhibition of Diffusion Flames by Methyl Bromide and Trifluoromethyl Bromide Applied to the Fuel and Oxygen Sides of the Reaction Zone." Journal of Research of the National bureau of Standards—*A. Physics and Chemistry* **65A**, No. 4, pp 389-396 (1961).
8. Hamins, A., Trees, D., Seshadri, K., and Chelliah, H.K. "Extinction of Nonpremixed Flames with Halogenated Fire Suppressants." *Combust. Flame* **99**:221-230 (1994).
9. Masri, A.R. "Chemical Inhibition of Nonpremixed Flames of Hydrocarbon Fuels with CF_3Br." *Comb. Sci. Tech.* **96**, pp 189-212 (1994).
10. Trees, D., Grudno, A., Ilincic, N., Weissweiler, T., and Seshadri, K. "Experimental and Numerical Studies on Chemical Inhibition of Methane-Air Diffusion Flames by CF_3Br and CF_3H." Presented at the Western States Meeting of the Combustion Institute, San Antonio, TX (1994).
11. Simmons, R.F. and Wolfhard, H.G. "The Influence of Methyl Bromide on Flames, Part 1 - Premixed Flames." *Trans. Far. Soc.* **51**, pp 1211-1217 (1955).
12. Simmons, R.F. and Wolfhard, H.G. "The Influence of Methyl Bromide on Flames, Part 2 - Diffusion Flames." *Trans. Far. Soc.* **52**, pp 53-59 (1956).
13. Price, D., Iddon, B., Wakefield, B.J., eds. "Bromine Compounds: Chemistry and Applications." Elsevier, Amsterdam (1988).
14. Ibiricu, M.M. and Gaydon, A.G. "Spectroscopic Studies of the Effect of Inhibitors on Counterflow Diffusion Flames." *Combust. Flame* **8**:51-62 (1964).
15. Seshadri, K. and Williams, F.A. "Effect of CF_3Br on Counterflow Combustion of Liquid Fuel with Diluted Oxygen." 'Halogenated Fire Suppressants', *ACS Symposium 16*, Am. Chem. Soc., Washington D.C., pp 149-179 (1975).
16. Vandooren, J. "The Inhibiting Effect of CF_3H on the Structure of a Stoichiometric $H_2/CO/O_2/Ar$ Flame." *Twenty-second Symposium (International) on Combustion*, The Combustion Institute. pp 1587-1595 (1988).
17. Linteris, G.T. "Acid Gas Production in Inhibited Propane-Air Diffusion Flames." Accepted for inclusion in *Halon Replacements: Technology and Science*, American Chemical Society Symposium Series (A.W. Mixiolek and W.Tsang, Eds.), Washington D.C. (1995).
18. Linteris, G.T. "Numerically Predicted Flame Structure and Burning Rates of Premixed CO-Ar-O2- H2 Flames Inhibited by CF3H," accepted for publication in *Combustion and Flame*, Jan. 1996.

19. Bahadori, M.Y., Edelman, R.B., Stocker, D.P., and Olson S.L. "Ignition and Behavior of Laminar Gas-Jet Diffusion Flames in Microgravity." *AIAA Journal* **28** (3), pp 236-244 (1989).
20. Bahadori, M.Y., Stocker, D.P., and Edelman, R.B. "Effects of Pressure on Microgravity Hydrocarbon Diffusion Flames." *AIAA Paper* 90-0651 (1990).
21. Bahadori, M.Y., Edelman, R.B., "Effects of Buoyancy of Gas Jet Diffusion Flame." NASA Contractor Report 191109 (1993).
22. Edelman, R.B. and Bahadori, M.Y. "Effects of Buoyancy on Gas-Jet Diffusion Flame: Experiment and Theory." *Acta Astronautica* **13** (11/12), pp 681-688 (1986).
23. Bahadori, M.Y., Edelman, R.B., Sotos, R.G., and Stocker, D.P. "Radiation from Gas-Jet Diffusion Flames in Microgravity Environments." *AIAA Paper* 91-0719 (1991).
24. Bahadori, M.Y., Edelman, R.B., Stocker, D.P., Sotos, R.G., and Vaughan, D.F. "Effects of Oxygen Concentration on Radiative Loss From Normal-Gravity and Microgravity Methane Diffusion Flames." *AIAA Paper* 92-0243 (1992).
25. Bahadori, M.Y., Stocker, D.P., Vaughan, D.F., Zhou, L., and Edelman, R.B. "Effects of Buoyancy on Laminar, Transitional, And Turbulent Gas Jet Diffusion Flames." Presented at the Second International Workshop on Combustion Science in Microgravity, Cleveland, OH (1992).
26. Koylu, U.O., Sunderland, P.B., Mortazavi, S., Faeth, G.M. "Soot Nucleation and Growth in Weakly-Buoyant Laminar Jet Diffusion Flames." *AIAA Paper* 94-0428 (1993).
27. Sunderland, P.B., Mortazavi, S., Faeth, G.M., Urban, D.L. "Laminar Smoke Points of Nonbuoyant Jet Diffusion Flames." *Combust. Flame* **96**:97-103 (1994)
28. Mortazavi, S., Sunderland, P.B., Jurng, J., Koylu, O.U., and Faeth, G.M. "Structure of Soot-Containing Laminar Jet Diffusion Flames." *AIAA Paper* 93-078 (1993).
29. Glassman, I. "Soot Formation in Combustion Processes." *Twenty-second Symposium (International) on Combustion*, pp 295-311 (1988).
30. Burgess, D.R.F., Jr., Zachariah, M.R., Tsang, W., Westmoreland, P.R. "Thermochemical and Chemical Kinetic Data for Fluorinated Hydrocarbons." NIST Technical Note 1412 (1995).
31. Schug, K.P., Manheimer-Timnat, Y., Yaccarino, P., Glassman, I. "Sooting Behavior of Gaseous Hydrocarbon Diffusion Flames and the Influence of Additives." *Comb. Sci. Tech.* **22**, pp 235-250 (1980).
32. Reynolds, W.C. STANJAN, Department of Mechanical Engineering, Stanford University (1986).
33. JANAF Thermochemical Tables, Dow Chemical Company, Clearinghouse, Springfield, VA.
34. Kee, R.J., Warnatz, J., and Miller, J.A., "A Fortran Computer Code Package for the Evaluation of Gas-Phase Viscosities, Conductivities, and Diffusion Coefficients," Sandia National Laboratories Report, SAND83-8209 (1983).

APPENDIX I

Test Conditions

Table AI.1 Experiment listing: Session 1

		Mole Fract.						
Code	Description*	CF_3Br (%)	CF_3H (%)	O_2 (%)	N_2 (%)	P (kPa)	Q_{fuel} (sccm)	Comments
1n1	ng - Baseline			21	79	101	154	Good
1n2	2% CF_3Br	2		20.6	77.4	101	154	Blew off
1n3	1% CH_4			20.8	78.2	101	154	Good
1n4	1% CF_3Br	1		20.8	78.2	101	154	Good
1n5	4% CF_3H		4	20.2	75.8	101	154	Good
1n6	8% CF_3H		8	19.3	72.7	101	154	Good
1n7								Failed
1n8	LP-Baseline			21	79	25	154	Use 1n10
1n9	95 torr			21	79	13	154	No ignition
1n10	LP-Baseline			21	79	25	154	Good
1n11	2% CF_3Br	2		20.6	77.4	101	154	Blew off
1n12	1% CF_3Br	1		20.8	78.2	25	154	Lifted
1n13	1.5% CF_3Br	1.5		20.7	77.8	101	154	Lifted
1n14	2% CF_3Br	2		20.6	77.4	25	154	Blew off
1u1	Test			21	79	101	??	Unknown flow rate
1u2	1% CF_3Br	1		20.8	78.2	101	154	Saturated
1u3,4								Failed
1u5	Baseline			21	79	101	154	Not fully developed
1u6								Failed
1u7	4% CF_3H		4	20.2	75.8	101	154	Unreliable (see 2u9)
1u8	2% CH_4			20.6	77.4	101	154	2% CH4;Not fully dev.
1u9	8% CF_3H		8	19.3	72.7	101	154	Good
1u10	12% CF_3H		12	18.5	69.5	101	154	Good
1u11	1.5% CF_3Br	1.5		20.7	77.8	101	154	Saturated
1u12	LP-1% CF_3Br	1		20.8	78.2	25	154	Good
1u13	LP-2% CF_3Br	2		20.6	77.4	25	154	Good

** LP: low pressure (25 kPa); HOC: high oxygen concentration (30%); LOC: low oxygen concentration (18%); HFR: high flow rate (308 sccm); CO: carbon monoxide/methane fuel; IF: inhibitor in fuel.*

Table AI.2 Experiment listing: Session 2

Code	Description*	Mole Fract. CF_3Br (%)	Mole Fract. CF_3H (%)	Mole Fract. O_2 (%)	Mole Fract. N_2 (%)	P (kPa)	Qfuel (sccm)	Comments
2u1								Failed
2u2	LP-Baseline			21	79	25	154	Good
2u3	8% CF_3H		8	19.3	72.7	101	154	Full camera gain; Good
2u4	8% CF_3H-21% O_2		8	21	71	101	154	Good
2u5	8% N2 dilution			19.3	80.7	101	154	Good
2u6	6% CF_3H		6	19.7	74.3	101	154	Good
2u7	LP-4% CF_3H		4	20.2	75.8	25	154	Good
2u8	LP-8% CF_3H		8	19.3	72.7	25	154	Good
2u9	5% CF_3H		5	20	75	101	154	Good
2u10	HOC-8% CF_3H		8	30	62	101	154	Saturated
2u11	HOC-LP-8% CF_3H		8	30	62	25	154	Good
2u12	HOC-12% CF_3H		12	30	58	101	154	Saturated
2u13	3% CF_3Br	3		20.4	76.6	101	154	Lit and extinguished
2u14	LOC-1% CF_3Br	1		18	81	101	154	Lit and extinguished
2u15	0.5% CF_3Br	0.5		20.9	78.6	101	154	Gain too low
2u16	Baseline			21	79	101	154	Good
2u17	LP-3% CF_3Br	3		20.4	76.6	25	154	No ignition
2u18	HOC-3% CF_3Br	3		30	67	101	154	Saturated
2u19	HOC-Baseline			30	70	101	154	Saturated

** LP: low pressure (25 kPa); HOC: high oxygen concentration (30%); LOC: low oxygen concentration (18%); HFR: high flow rate (308 sccm); CO: carbon monoxide/methane fuel; IF: inhibitor in fuel.*

Table AI.3 Experiment listing: Session 3

		Mole Fract.						
Code	Description*	CF_3Br (%)	CF_3H (%)	O_2 (%)	N_2 (%)	P (kPa)	Qfuel (sccm)	Comments
3u1	Baseline			21	79	101	154	Unreliable (see 2u16)
3u2	18% O2			18	82	101	154	Good
3u3	1% CF_3Br	1		20.8	78.2	101	154	Good
3u4	2% CF_3Br	2		20.6	77.4	101	154	Saturated
3u5	HFR-Base			21	79	101	308	Gain too low
3u6	HFR-1% CF_3Br	1		20.8	78.2	101	308	Gain too low
3u7	HFR-2% CF_3Br	2		20.6	77.4	101	308	Saturated
3u8	HFR-8% CF_3H		8	19.3	72.7	101	308	Gain too low
3u9	15% CF_3H		15	17.8	67.2	101	154	Lit and extinguished
3u10	2% CF_3H		2	20.6	77.4	101	154	Good
3u11	HFR-15% CF_3H		15	17.8	67.2	101	308	Gain too low
3u12	1% CF_3H		1	20.8	78.2	101	154	Good
3u13	CO-Base			21	79	101	308	Unreliable (see 3u14)
3u14	CO-Base			21	79	101	308	Good
3u15	CO-8% CF_3H		8	19.3	72.7	101	308	No ignition
3u16	CO-2% CF_3H		2	20.6	77.4	101	308	Good
3u17	CO-4% CF_3H		4	20.2	75.8	101	308	No ignition
3u18	CO-3% CF_3H		3	20.4	76.6	101	308	Blew off
3u19	CO-LP			21	79	25	308	No ignition
3u20	CO-2% CF_3H		2	20.6	77.4	101	308	Blew off
3u21	CO-0.5% CF_3Br	0.5		20.9	78.6	101	308	Blew off
3u22	CO-0.5% CF_3Br	0.5		20.9	78.6	101	154	Gain too low
3u23	CO-0.5% CF_3Br	0.5		20.9	78.6	101	154	Good
3u24	CO-Base-154			21	79	101	154	Good
3u25	IF-5%CF_3Br			21	79	101	154	Inh. in fuel; Gain low
4n1	4% CF_3H		4	20.4	75.6	25	154	Good

** LP: low pressure (25 kPa); HOC: high oxygen concentration (30%); LOC: low oxygen concentration (18%); HFR: high flow rate (308 sccm); CO: carbon monoxide/methane fuel; IF: inhibitor in fuel.*

Table AI.4 Reynolds and Froude numbers

Fuel	Flow Rate (sccm)	Pressure (kPa)	Re*	Fr**
CH_4	154	101	120	77
CH_4	308	101	240	306
CH_4	154	25	120	1226
CO	154	101	159	77
CO	308	101	258	306

* *Reynolds number: Re = UD/v, where U is jet velocity, D is jet diameter, and n is kinematic viscosity.*

** *Froude number: Fr = U^2/gD. where g is acceleration of gravity.*

Table AI.5 Gas properties

Species	Molecular Weight (kg/kmol)	Specific Heat* (kJ/kmol-K)	Specific Heat* (kJ/kg-K)
N_2	28.01	29.07	1.038
O_2	32.00	29.31	0.916
CF_3H	70.02	51.15	0.731
CF_3Br	148.92	69	0.463

* *From [30], except CF_3Br from [1].*

APPENDIX II

Selected Flame Images

The intensity of the images presented here are not directly comparable due to changes in the camera gain required to obtain satisfactory contrast.

Table AII.1 Scale of digitized video

Series	Conversion	Scale *(pixels/mm)*
1	4" = 315 pixels	3.1
2	100 mm = 527 pixels	5.27
3u1-15	100 mm = 545 pixels	5.45
3u16-25	80 mm = 579 pixels	7.24

Table AII.2 Image cross reference

Exp. Code	Figure	Page
1n1	AII.1	51
1n10	AII.1	51
	AII.8	58
1n12	AII.8	58
1u10	AII.4	54
1u11	AII.2	52
1u12	AII.9	59
1u13	AII.9	59
2u2	AII.1	51
	AII.9	59
2u3	AII.4	54
	AII.5	55
2u4	AII.5	55
2u5	AII.5	55
2u6	AII.4	54
2u7	AII.9	59
2u8	AII.9	59
2u9	AII.4	54
2u10	AII.6	56
2u12	AII.6	56
2u13	AII.2	52
2u14	AII.3	53
2u16	AII.1	51
	AII.2	52
	AII.4	54
	AII.5	55
2u18	AII.6	56
2u19	AII.1	51
	AII.6	56
3u2	AII.5	55
3u3	AII.2	52
3u4	AII.2	52
3u5	AII.7	57
3u6	AII.7	57
3u7	AII.7	57
3u8	AII.7	57
3u11	AII.7	57
3u12	AII.4	54
3u14	AII.10	60
3u16	AII.10	60
3u23	AII.10	60
3u24	AII.1	51
	AII.10	60
4n1	AII.8	58

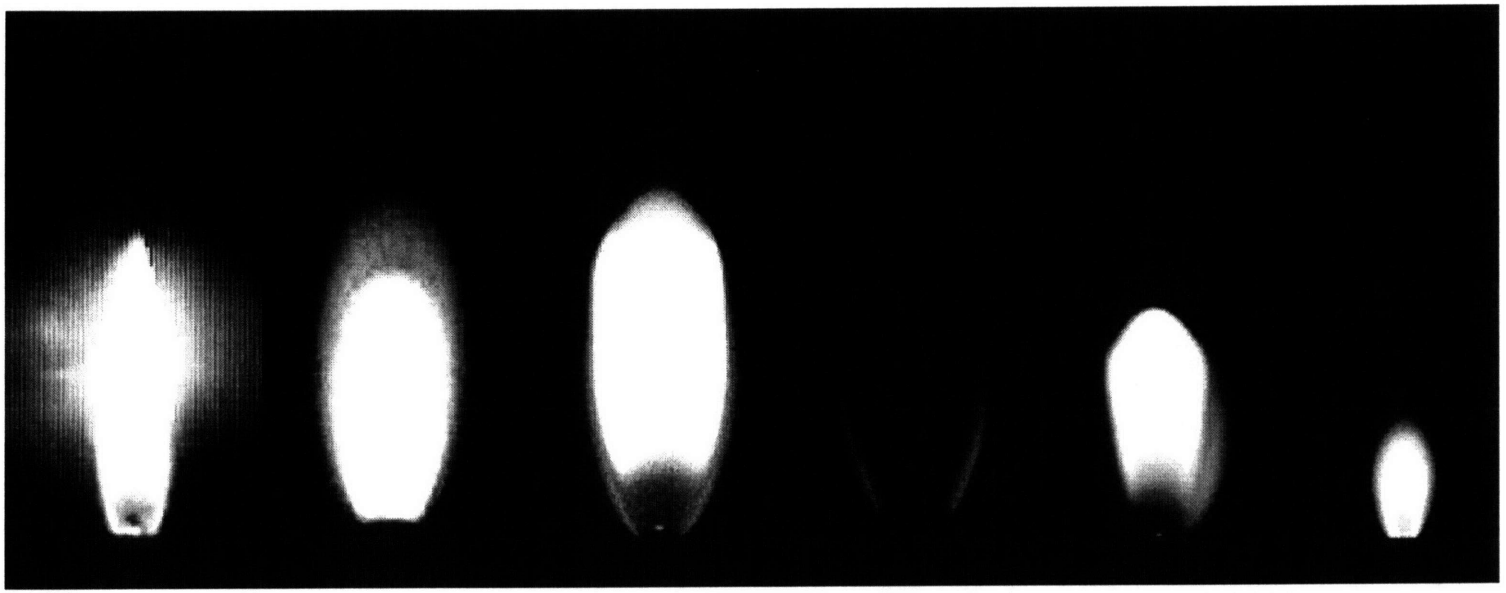

Figure AII.1 Images of uninhibited flames; 154 sccm. (1n1) ng, CH_4 fuel, 101 kPa, substantial flicker, sooty. (1n10) ng, CH_4 fuel, 25 kPa, no flicker, all blue. (2u16) μg, CH_4 fuel, 101 kPa, blue base and edges, sooty core. (2u2) μg, CH_4 fuel, 25 kPa, all blue. (2u19) μg, CH_4 fuel, 30% O_2, 101 kPa, sooty core. (3u24) μg, CO fuel, 101 kPa, all blue.

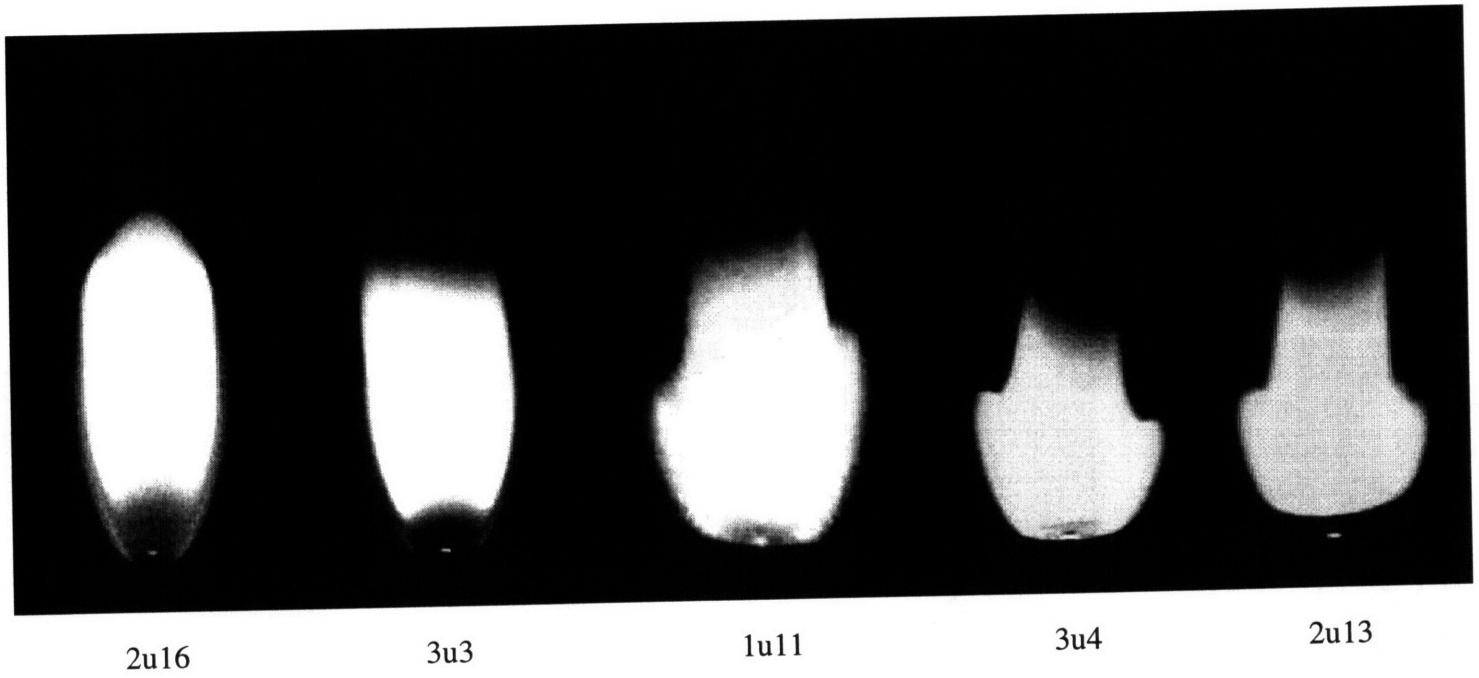

Figure AII.2 Images of CF_3Br flame inhibition; microgravity, 101 kPa, 154 sccm CH_4. (2u16) uninhibited, blue sides and base. (3u3) 1% CF_3Br, blue visible at base aligned with interface of zones, sooty inner region, orange outer region. (1u11) 1.5% CF_3Br, mostly saturated, orange to red at sides and tip. (3u4) 2% CF_3Br, mostly saturated, orange to red at sides and tip. (2u13) 3% CF_3Br, 0.17 seconds prior to extinction, mostly saturated, orange to red at sides and tip.

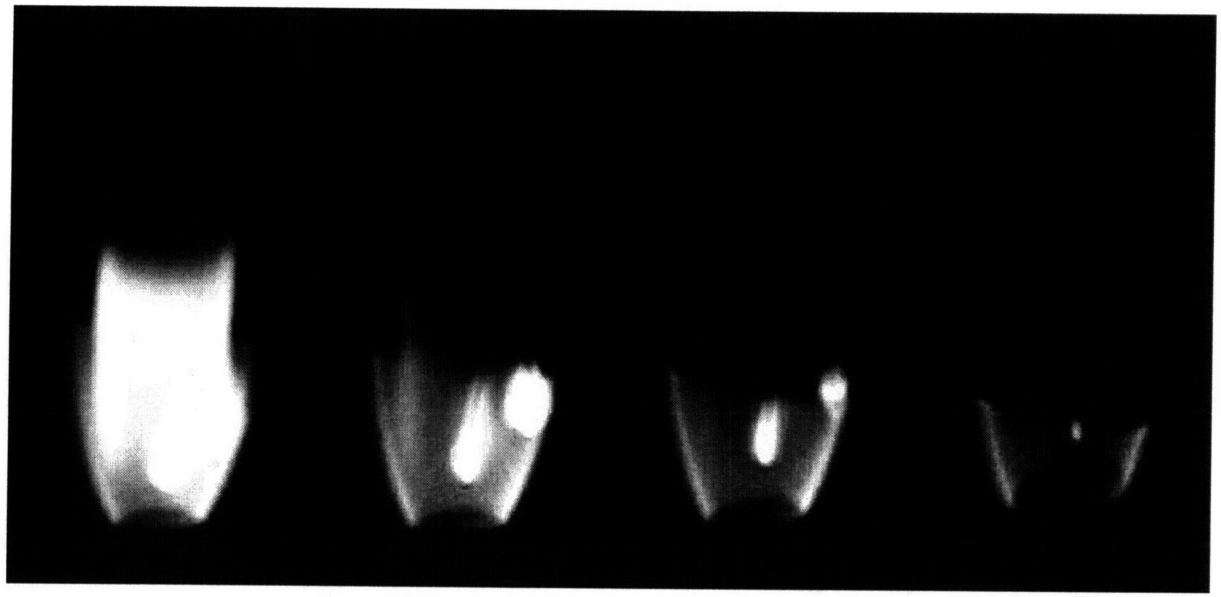

2u14a 2u14b 2u14c 2u14d

Figure AII.3 Images of extinction transient for 1% CF_3Br / 18% O_2 flame; microgravity, 101 kPa, 154 sccm CH_4. Sooty inner zone, blue surrounded by orange outer shell. Bright spots are pieces of ignitor wire. (2u14a) frame 13:16, 0.30 sec. after ignition. (2u14b) frame 13:17, 0.33 sec. after ignition. (2u14c) frame 13:19, 0.40 sec. after ignition. (2u14d) frame 13:23, 0.53 sec. after ignition, extinction 0.13 sec. later.

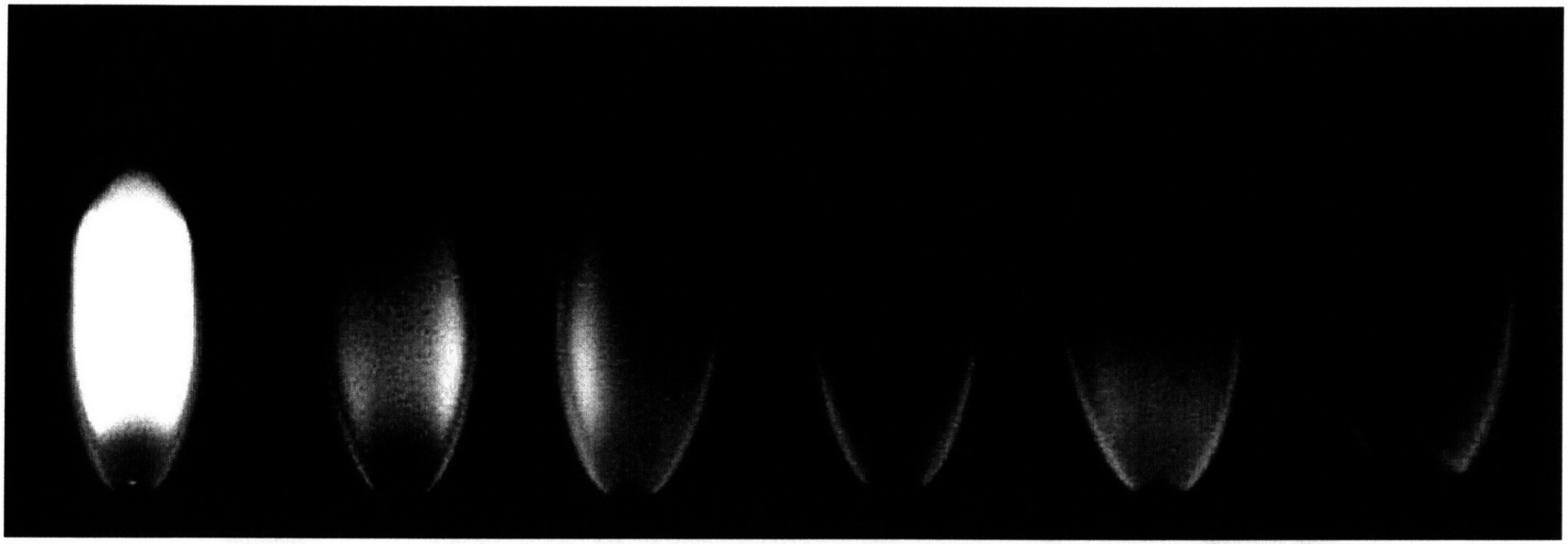

Figure AII.4 Images of CF_3H flame inhibition; microgravity, 101 kPa, 154 sccm CH_4. (2u16) uninhibited, blue base and sides, sooty core. (3u12) 1% CF_3H, blue shell with soot in interior. (2u9) 5% CF_3H, blue shell with a little soot. (2u6) 6% CF_3H, all blue. (2u3) 8% CF_3H, all blue. (1u10) 12% CF_3H, all blue.

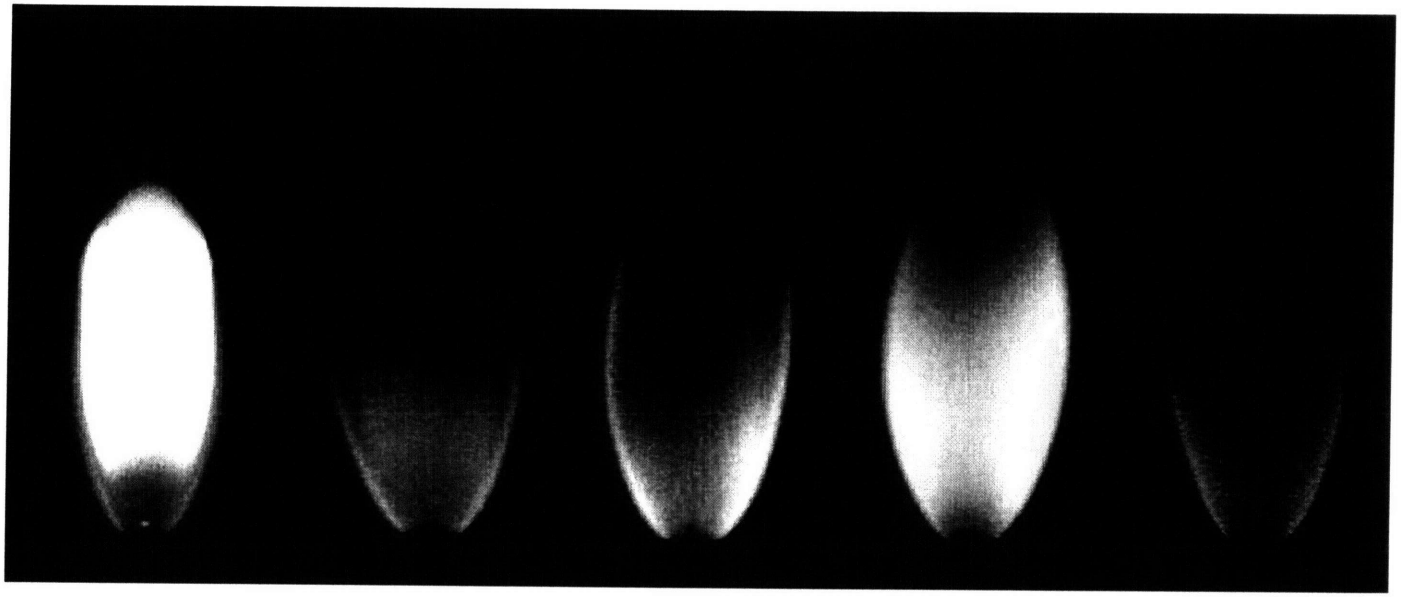

Figure AII.5 Images of dilution effect in flames; microgravity, 101 kPa, 154 sccm CH_4. (2u16) uninhibited, blue base and sides, sooty core. (2u3) 8% CF_3H, all blue. (2u4) 8% CF_3H / 21% O_2, all whitish-blue. (2u5) 8% N_2 dilution, blue shell with some soot inside. (3u2) 14.3% N_2 dilution, all violet-blue.

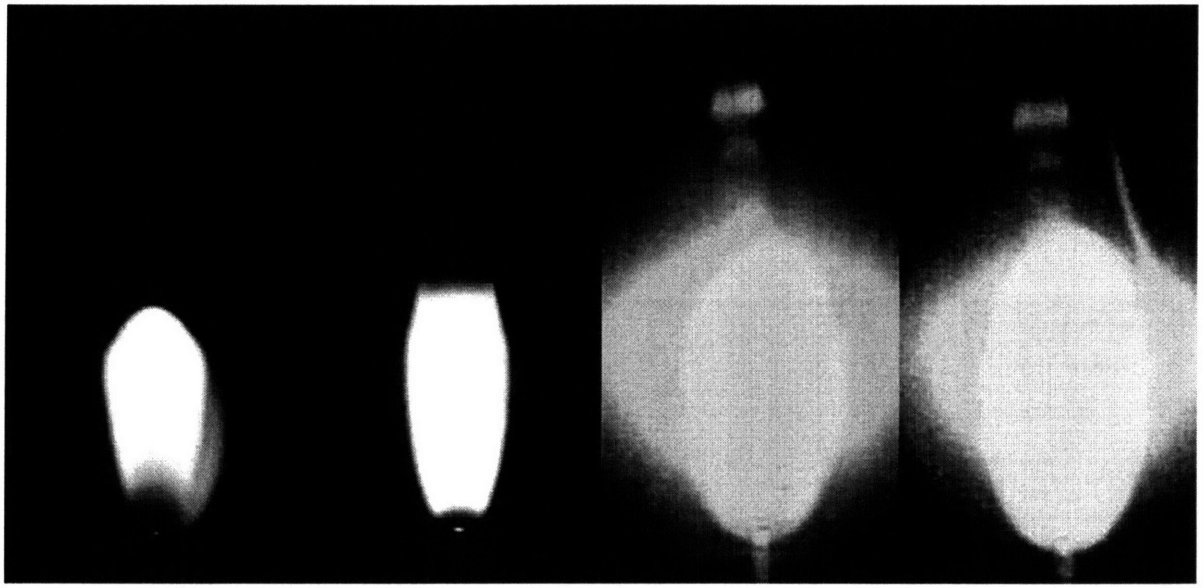

2u19 2u18 2u10 2u12

Figure AII.6 Images of the effect of increased oxygen concentration on flames; 30% O_2, 101 kPa, 154 sccm CH_4. (2u19) uninhibited, sooty core. (2u18) 3% CF_3Br, very thick and dim reddish outer zone. (2u10) 8% CF_3H, image saturated. (2u12) 12% CF_3H, image saturated.

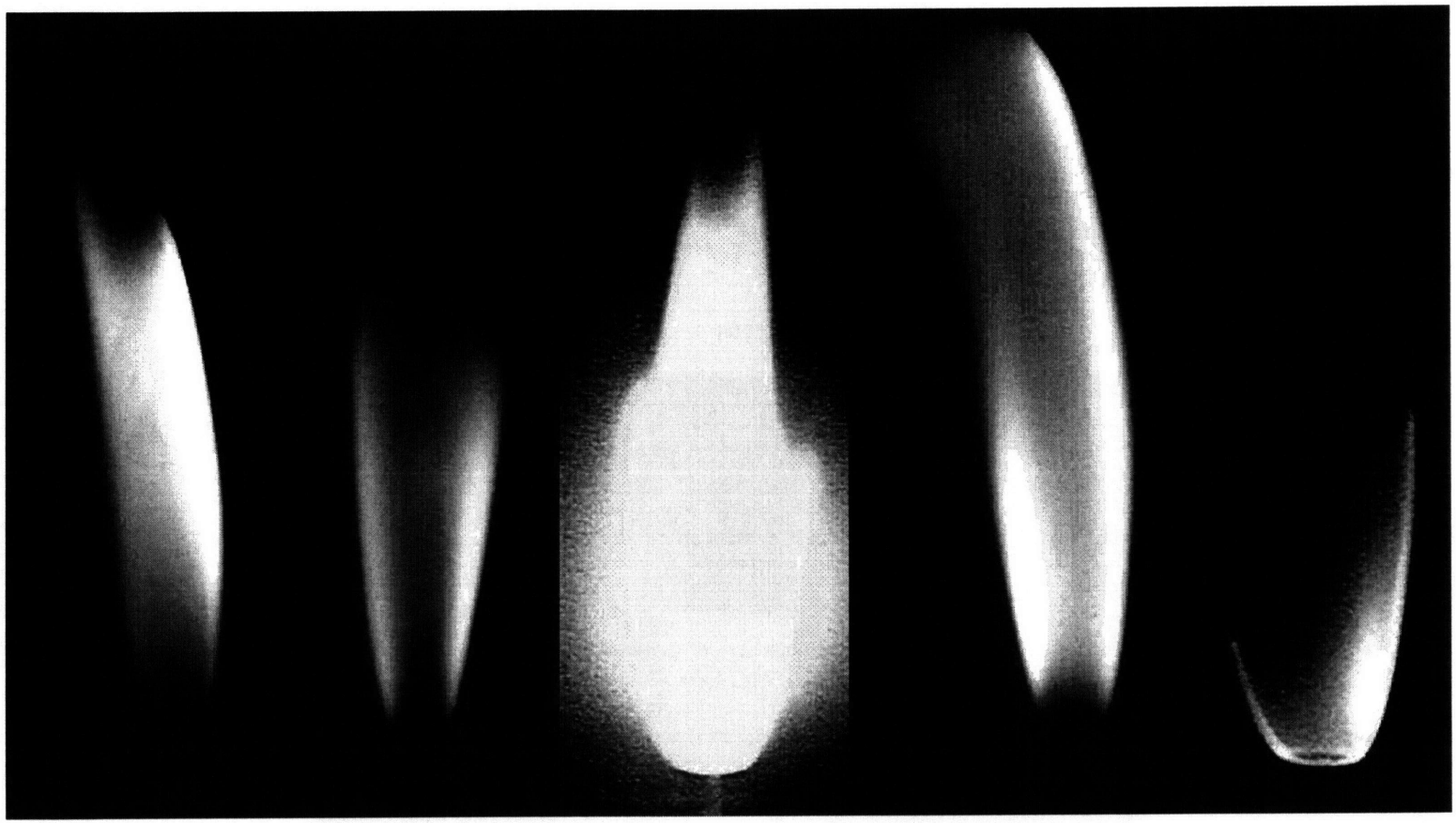

Figure AII.7 Images of flames at higher flow rate; microgravity, 101 kPa, 308 sccm CH_4. (3u5) uninhibited, only soot visible. (3u6) 1% CF_3Br, only soot visible. (3u7) 2% CF_3Br, image saturated. (3u8) 8% CF_3H, blue shell with sooty interior. (3u11) 15% CF_3H, all blue.

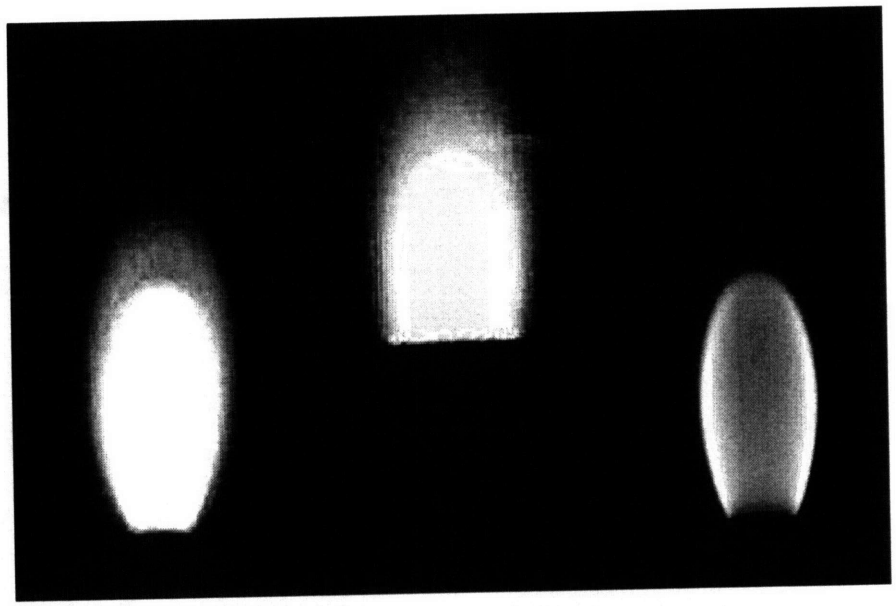

Figure AII.8 Image of low-pressure, normal-gravity flames; 25 kPa, 154 sccm CH_4. (1n10) uninhibited, halo blue, center saturated. (1n12) 1% CF_3Br, saturated center, blue halo turning to red tail. (4n1) 4% CF_3H, blue center and halo, lower gain than 1n10.

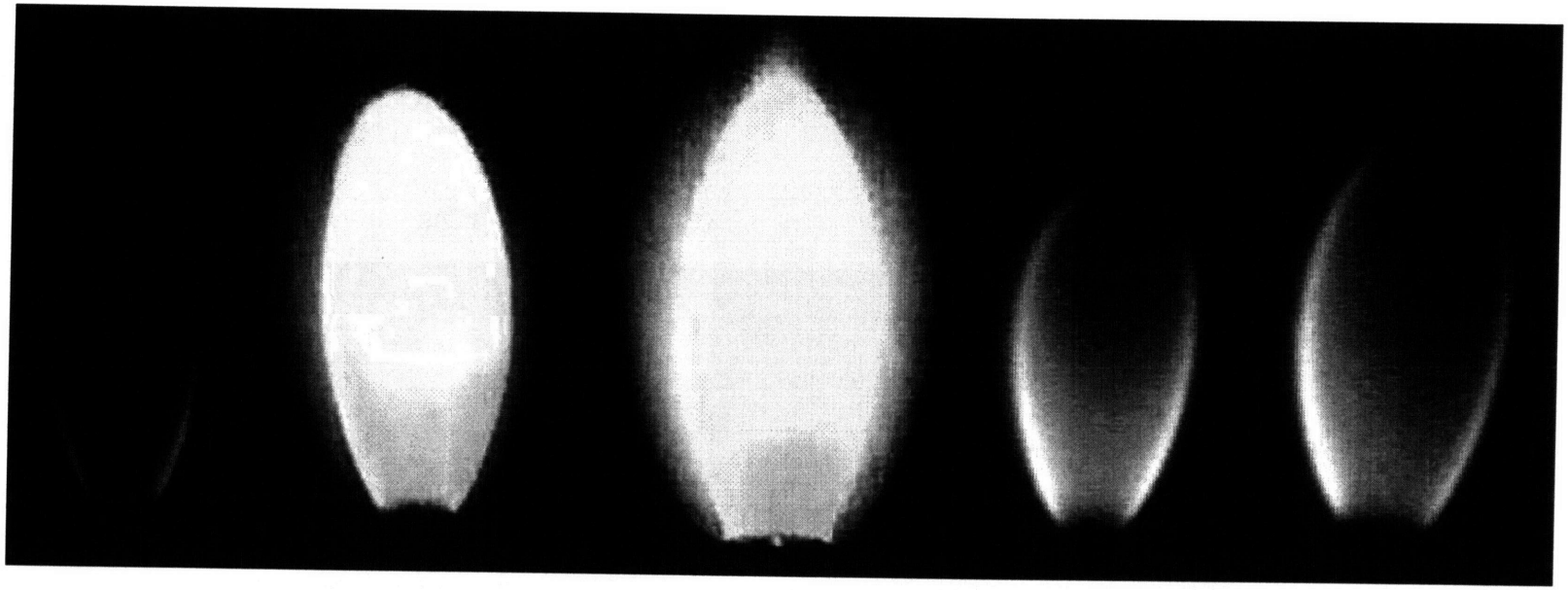

Figure AII.9 Images of low-pressure, microgravity flames; 25 kPa, 154 sccm CH_4. (2u2) uninhibited, all blue, low gain. (1u12) 1% CF_3Br, greenish base, sooty upper half, orange halo. (1u13) 2% CF_3Br, greenish base, upper 2/3 sooty, orange halo. (2u7) 4% CF_3H, all blue. (2u8) 8% CF_3H, all blue.

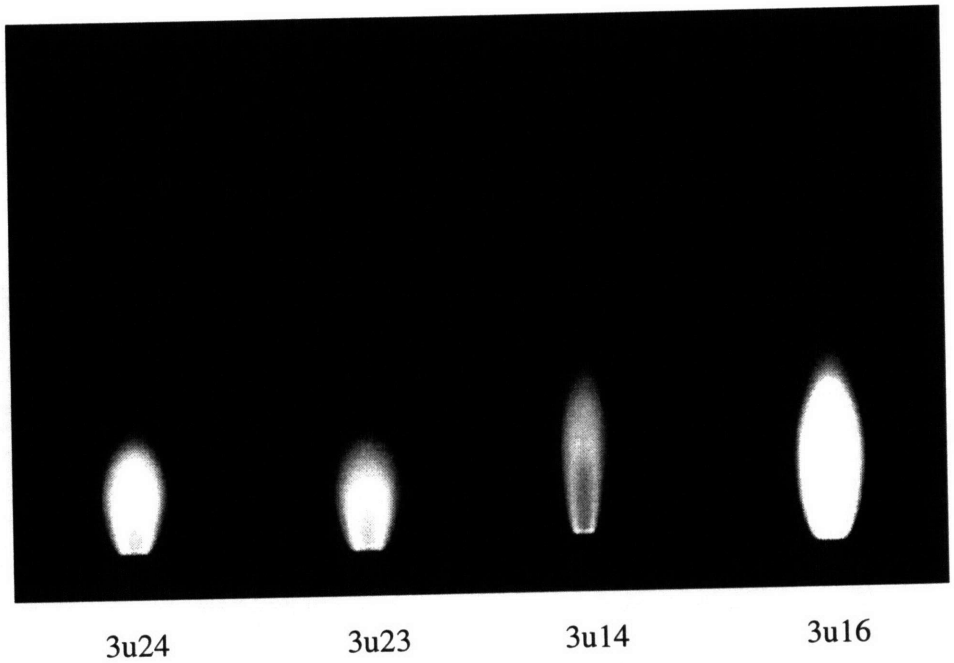

Figure AII.10 Images of carbon monoxide flames in microgravity; 1% CH_4 in fuel, microgravity, 101 kPa. (3u24) 154 sccm, uninhibited, all blue. (3u23) 154 sccm, 0.5% CF_3Br, all blue. (3u14) 308 sccm, uninhibited, all blue. (3u16) 308 sccm, 2% CF_3H, image saturated.

Table AII.3 Microgravity flame characteristics

Code	Description: Inhibition	xO_2 (%)	P (kPa)	Q_{fuel} (sccm)	Flame: Length (mm)	Flame: Width (mm)	Soot	Tip	Soot Plume: Length (mm)	Soot Plume: Width (mm)
CF_3Br Addition										
2u15	0.5% CF_3Br	20.9	101	154	??	??	yes	open	36	17
3u3	1% CF_3Br	20.8	101	154	28	23	yes	open	39	19
1u11	1.5% CF_3Br	20.7	101	154	25	27	yes	open	34	17
3u4	2% CF_3Br	20.6	101	154	17	23	yes	open	34	16
2u13	3% CF_3Br	20.4	101	154	<<< EXTINCTION >>>					
2u14	1% CF_3Br	18	101	154	<<< EXTINCTION >>>					
CF_3H Addition										
3u12	1% CF_3H	20.8	101	154	43	24	yes	open	- -	- -
3u10	2% CF_3H	20.6	101	154	44	24	yes	open	- -	- -
2u9	5% CF_3H	20.0	101	154	48	23	yes	open	- -	- -
2u6	6% CF_3H	19.7	101	154	37	25	no	open	- -	- -
2u3	8% CF_3H	19.3	101	154	34	27	no	open	- -	- -
1u10	12% CF_3H	18.5	101	154	35	29	no	open	- -	- -
3u9	15% CF_3H	17.8	101	154	<<< EXTINCTION >>>					
2u4	8% CF_3H	21	101	154	42	24	no	open	- -	- -
Varied Oxygen Concentration										
3u2	None	18	101	154	42	27	no	open	- -	- -
2u5	None	19.3	101	154	50	23	yes	closed	- -	- -
2u16	None	21	101	154	45	22	yes	closed	- -	- -
2u19	None	30	101	154	29	15	yes	closed	- -	- -
2u18	3% CF_3Br	30	101	154	32	13	yes	open	- -	- -
2u10	8% CF_3H	30	101	154	37	20	yes	closed	- -	- -
2u12	12% CF_3H	30	101	154	39	20	yes	closed	- -	- -
High Flow Rate										
3u5	None	21	101	308	95	??	yes	closed	95	17
3u6	1% CF_3Br	20.8	101	308	78	24	yes	closed	- -	- -
3u7	2% CF_3Br	20.6	101	308	46	26	yes	open	97	16
3u8	8% CF_3H	19.3	101	308	??	??	yes	??	108	23
3u11	15% CF_3H	17.8	101	308	60	28	no	open	- -	- -
Low Pressure										
2u2	None	21	25	154	35	20	no	closed	- -	- -
1u12	1% CF_3Br	20.8	25	154	53	25	yes	closed	- -	- -
1u13	2% CF_3Br	20.6	25	154	60	26	yes	closed	- -	- -
2u7	4% CF_3H	20.2	25	154	47	24	no	closed	- -	- -
2u8	8% CF_3H	19.3	25	154	53	26	no	closed	- -	- -
CO Fuel										
3u24	None	21	101	154	16	9	no	closed	- -	- -
3u23	0.5% CF_3Br	20.9	101	154	17	10	no	closed	- -	- -
3u14	None	21	101	308	25	7	no	closed	- -	- -
3u16	2% CF_3H	20.6	101	308	27	9	no	closed	- -	- -

APPENDIX III

Equilibrium Calculations

This section described equilibrium calculations performed as a first-order analysis of flame composition. The stoichiometry of the reaction is calculated assuming equal diffusion rates of all species to the flame. This assumption allows the mole fractions in the oxidizer to be the same at the flame as in the far field. The flame is assumed to consume fuel and oxidizer mixture in a ratio which will allow complete conversion to the most stable products. The set of products used depends on the ratio of H atoms to F atoms in the system.

Stoichiometric reaction for the case of ($n_H > n_F$);

$$a\,CH_4 + b\,CF_3H + c\,(O_2 + 3.76\,N_2) \text{ fi } d\,CO_2 + e\,H_2O + f\,HF + 3.76\,c\,N_2$$

C: $a + b = d$

H: $4a + b = 2e + f$

O: $2c = 2d + e$

F: $3b = f$

Solving for a = a(b,c);

$$a = -0.25\,b + 0.5\,c$$

Stoichiometric reaction for the case of ($n_F > n_H$);

$$a\,CH_4 + b\,CF_3H + c\,(O_2 + 3.76\,N_2) \text{ fi } d\,CO_2 + e\,CF_2O + f\,HF + 3.76\,c\,N_2$$

C: $a + b = d + e$

H: $4a + b = f$

O: $2c = 2d + e$

F: $3b = 2e + f$

Which gives the same equation for stoichiometry.

Ratio of inhibitor to air taken from mole fraction in far field;

$$[CF_3H] = \frac{b}{(b + 4.76c)}$$

$$b[CF_3H] + 4.76c[CF_3H] = b$$

$$b = \frac{4.76c[CF_3H]}{1 - [CF_3H]}$$

Next, the concentration of inhibitor at which (H = F) is informative;

$$4a + b = 3b$$
$$a = 0.5\,b$$

$$0.5\,b = -0.25\,b + 0.5\,c$$
$$b = 2/3\,c$$

$$[CF_3H] = \frac{2/3}{2/3 + 4.76} = 0.123 = 12.3\%$$

Taking $c = 1$,
$b = 0.668$
$a = 0.333$

The resultant ratios of moles of reactant are then used as the input state at a temperature of 298 K and a pressure of 101 kPa. STANJAN [32,33] is then used to calculate the equilibrium state at constant pressure and enthalpy.

Table AIII.1 shows the specific heats of oxidizer mixtures used in the experiments. Table AIII.2 shows the moles of reactants used in the equilibrium calculations and the resulting temperature.

Table AIII.1 Oxidizer mixture properties

UNINHIBITED		Oxidizer Mass Fraction			Oxidizer Mass Averaged	
					M	Cp
xN_2 dil	xO_2	yO_2	yN_2		*(kg/kmol)*	*(kJ/kmolK)*
0.143	0.18	0.200	0.800		28.81	29.20
0.08	0.1932	0.215	0.785		28.87	29.20
	0.21	0.233	0.767		28.94	29.21
	0.3	0.329	0.671		29.32	29.26
REPLACING AIR						
xCF_3H	xO_2	yO_2	yN_2	yCF_3H	M	Cp
0	0.21	0.233	0.767	0.000	28.94	29.21
0.01	0.208	0.227	0.749	0.024	29.92	30.01
0.02	0.206	0.222	0.731	0.047	30.88	30.76
0.04	0.202	0.212	0.697	0.092	32.71	32.18
0.05	0.200	0.207	0.680	0.113	33.59	32.85
0.06	0.197	0.202	0.664	0.134	34.45	33.49
0.08	0.193	0.192	0.633	0.174	36.10	34.68
0.12	0.185	0.175	0.576	0.249	39.16	36.81
0.15	0.179	0.163	0.537	0.3	41.26	38.20
xCF_3Br	xO_2	yO_2	yN_2	yCF_3Br	M	Cp
0	0.21	0.233	0.767	0.000	28.94	29.21
0.005	0.209	0.227	0.748	0.025	31.98	31.83
0.01	0.208	0.221	0.729	0.050	34.89	34.27
0.015	0.207	0.216	0.711	0.073	37.68	36.54
0.02	0.206	0.211	0.694	0.095	40.38	38.65
0.03	0.204	0.201	0.661	0.138	45.46	42.47
SET OXYGEN FRACTION						
xCF_3H	xO_2	yO_2	yN_2	yCF_3H	M	Cp
0.08	0.21	0.209	0.617	0.174	36.15	34.66
0.08	0.3	0.295	0.533	0.172	36.41	34.56
0.12	0.3	0.280	0.474	0.245	39.44	36.61
xCF_3Br	xO_2	yO_2	yN_2	yCF_3Br	M	Cp
0.01	0.18	0.192	0.758	0.050	34.79	34.30
0.03	0.3	0.292	0.572	0.136	45.63	42.16

Table AIII.2 Equilibrium calculation parameters

UNINHIBITED xN_2 dil	xO_2	nO_2	nN_2		nCH_4	Equil. Temp. (K)
0.143	0.18	1	4.556		0.5	2068
0.08	0.1932	1	4.176		0.5	2144
	0.21	1	3.762		0.5	2230
	0.3	1	2.333		0.5	2534
REPLACING AIR						
xCF_3H	xO_2	nO_2	nN_2	nCF_3H	nCH_4	Temp.
0	0.21	1	3.76	0.000	0.500	2230
0.01	0.208	1	3.76	0.048	0.488	2220
0.02	0.206	1	3.76	0.097	0.476	2209
0.04	0.202	1	3.76	0.198	0.450	2187
0.05	0.200	1	3.76	0.251	0.437	2177
0.06	0.197	1	3.76	0.304	0.424	2166
0.08	0.193	1	3.76	0.414	0.397	2146
0.12	0.185	1	3.76	0.649	0.338	2106
0.15	0.179	1	3.76	0.840	0.290	1951
xCF_3Br	xO_2	nO_2	nN_2	nCF_3Br	nCH_4	Temp.
0	0.21	1	3.76	0.000	0.5	2230
0.005	0.209	1	3.76	0.024	0.5	2221
0.01	0.208	1	3.76	0.048	0.5	2211
0.015	0.207	1	3.76	0.072	0.5	2201
0.02	0.206	1	3.76	0.097	0.5	2191
0.03	0.204	1	3.76	0.147	0.5	2170
SET OXYGEN FRACTION						
xCF_3H	xO_2	nO_2	nN_2	nCF3H	nCH_4	Temp.
0.08	0.21	1	3.381	0.381	0.405	2226
0.08	0.3	1	2.067	0.267	0.433	2516
0.12	0.3	1	1.933	0.400	0.400	2510
xCF_3Br	xO_2	nO_2	nN_2	nCF_3Br	nCH_4	Temp.
0.01	0.18	1	4.500	0.056	0.5	2059
0.03	0.3	1	2.233	0.100	0.5	2506
CO/CH4 FUEL						
xCF_3H	xO_2	nO_2	nN_2	nCF_3H	nCO/CH_4	Temp.
0	0.21	1	3.76	0.000	1.942	2386
0.02	0.206	1	3.76	0.097	1.848	2293
xCF_3Br	xO2	nO2	nN2	nCF_3Br	nCO/CH4	Temp.
0.005	0.209	1	3.76	0.024	1.942	2380

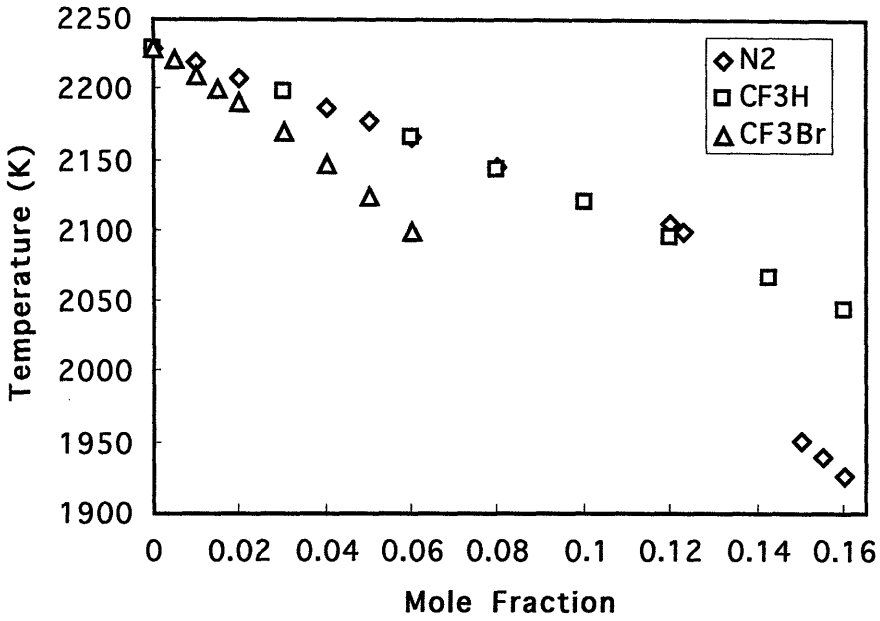

Figure AIII.1 Stoichiometric equilibrium temperature with addition of nitrogen and inhibitors. Methane fuel; additive in air; initial temperature 298 K; pressure 101 kPa. Solutions could not be found between 12.3 and 15% CF_3H addition.

Table AIII.3 Equilibrium sample outputs

Sample	Fuel	Inhibition	Page
1	CH_4	uninhibited	68
2	CH_4	8% N_2 dilution	70
3	CH_4	8% CF_3H	72
4	CH_4	8% CF_3H / 21% O_2	74
5	CH_4	15% CF_3H	76
6	CH_4	3% CF_3Br	78
7	CO	uninhibited	80

SAMPLE 1: Uninhibited

```
 CKLIB:  Chemical Kinetics Library
         CHEMKIN-II Version 4.1, February 1993
         DOUBLE PRECISION

          KEYWORD INPUT

CONH
CONP
REAC O2      1.
REAC N2      3.762
REAC CH4     0.5
REAC CHF3    0.
REAC CF3BR   0.
TEMP   298.
PRES   1.
END

 Constant pressure and enthalpy problem:

EQUIL:  Chemkin interface for Stanjan-III
        CHEMKIN-II Version 3.0, December 1992
        DOUBLE PRECISION

        WORKING SPACE REQUIREMENTS
            PROVIDED          REQUIRED
INTEGER             5000              2387
REAL                5000              4119
 STANJAN:  Version 3.8C, May 1988
           W. C. Reynolds, Stanford Univ.

                    INITIAL STATE:      EQUILIBRIUM STATE:
P (atm)               1.0000E+00          1.0000E+00
T (K)                 2.9800E+02          2.2299E+03
V (cm3/gm)            8.8486E+02          6.6698E+03
H (erg/gm)           -2.5663E+09         -2.5663E+09
U (erg/gm)           -3.4629E+09         -9.3244E+09
S (erg/gm-K)          7.2401E+07          9.8734E+07
W (gm/mole)           2.7633E+01          2.7433E+01


Mole Fractions
H2                    0.0000E+00          3.4599E-03
H                     0.0000E+00          3.9166E-04
O                     0.0000E+00          2.3699E-04
O2                    1.9004E-01          5.2908E-03
OH                    0.0000E+00          3.0255E-03
H2O                   0.0000E+00          1.8350E-01
HO2                   0.0000E+00          5.6031E-07
H2O2                  0.0000E+00          4.9549E-08
C                     0.0000E+00          2.1874E-17
CH                    0.0000E+00          3.2068E-18
CH2                   0.0000E+00          8.9842E-18
CH2SING               0.0000E+00          5.4672E-19
CH3                   0.0000E+00          5.4328E-17
CH4                   9.5021E-02          2.5355E-17
CO                    0.0000E+00          8.6765E-03
CO2                   0.0000E+00          8.5657E-02
HCO                   0.0000E+00          7.6451E-10
CH2O                  0.0000E+00          1.2240E-11
CH2OH                 0.0000E+00          3.7787E-17
CH3O                  0.0000E+00          6.0603E-19
```

CH3OH	0.0000E+00	3.0817E-18
C2H	0.0000E+00	3.1920E-24
C2H2	0.0000E+00	7.5194E-22
C2H3	0.0000E+00	5.6156E-27
C2H4	0.0000E+00	5.6005E-27
C2H5	0.0000E+00	5.9962E-32
C2H6	0.0000E+00	4.1788E-33
HCCO	0.0000E+00	4.7895E-20
CH2CO	0.0000E+00	6.0699E-20
HCCOH	0.0000E+00	6.0380E-23
N2	7.1494E-01	7.0976E-01
AR	0.0000E+00	0.0000E+00
H2CCCH	0.0000E+00	0.0000E+00
C4H2	0.0000E+00	0.0000E+00
C3H2	0.0000E+00	1.9759E-33
HCCHCCH	0.0000E+00	0.0000E+00
HF	0.0000E+00	0.0000E+00
F	0.0000E+00	0.0000E+00
CH3F	0.0000E+00	0.0000E+00
CH2F2	0.0000E+00	0.0000E+00
CHF3	0.0000E+00	0.0000E+00
CF4	0.0000E+00	0.0000E+00
CH2F	0.0000E+00	0.0000E+00
CHF2	0.0000E+00	0.0000E+00
CF3	0.0000E+00	0.0000E+00
CHF	0.0000E+00	0.0000E+00
CF2	0.0000E+00	0.0000E+00
CF	0.0000E+00	0.0000E+00
CF3O	0.0000E+00	0.0000E+00
CHF:O	0.0000E+00	0.0000E+00
CF2:O	0.0000E+00	0.0000E+00
CF:O	0.0000E+00	0.0000E+00
CF2CO	0.0000E+00	0.0000E+00
FCCO-E	0.0000E+00	0.0000E+00
CH3-CF2	0.0000E+00	0.0000E+00
CHF2-CH2	0.0000E+00	0.0000E+00
CH2:CF2	0.0000E+00	0.0000E+00
CH2:CHF	0.0000E+00	0.0000E+00
CF2:CH	0.0000E+00	0.0000E+00
C2HF	0.0000E+00	0.0000E+00
CF3-CF3	0.0000E+00	0.0000E+00
BR	0.0000E+00	0.0000E+00
BR2	0.0000E+00	0.0000E+00
HBR	0.0000E+00	0.0000E+00
CF3BR	0.0000E+00	0.0000E+00
CH3BR	0.0000E+00	0.0000E+00
CH2:CHBR	0.0000E+00	0.0000E+00
CH3-CH2BR	0.0000E+00	0.0000E+00
C2H3BR	0.0000E+00	0.0000E+00
C2H5BR	0.0000E+00	0.0000E+00
FBR	0.0000E+00	0.0000E+00
BRO	0.0000E+00	0.0000E+00
HOBR	0.0000E+00	0.0000E+00

SAMPLE 2: 8% Nitrogen dilution

```
 CKLIB:  Chemical Kinetics Library
         CHEMKIN-II Version 4.1, February 1993
         DOUBLE PRECISION

          KEYWORD INPUT

CONH
CONP
REAC O2      1.
REAC N2      4.176
REAC CH4     0.5
REAC CHF3    0.
REAC CF3BR   0.
TEMP   298.
PRES   1.
END

 Constant pressure and enthalpy problem:

EQUIL:  Chemkin interface for Stanjan-III
        CHEMKIN-II Version 3.0, December 1992
        DOUBLE PRECISION

        WORKING SPACE REQUIREMENTS
            PROVIDED          REQUIRED
INTEGER             5000              2387
REAL                5000              4119
 STANJAN:  Version 3.8C, May 1988
           W. C. Reynolds, Stanford Univ.

                    INITIAL STATE:       EQUILIBRIUM STATE:
P (atm)               1.0000E+00           1.0000E+00
T (K)                 2.9800E+02           2.1440E+03
V (cm3/gm)            8.8398E+02           6.3898E+03
H (erg/gm)           -2.3768E+09          -2.3768E+09
U (erg/gm)           -3.2725E+09          -8.8513E+09
S (erg/gm-K)          7.2172E+07           9.7483E+07
W (gm/mole)           2.7661E+01           2.7533E+01


Mole Fractions
H2                    0.0000E+00           2.3170E-03
H                     0.0000E+00           1.9608E-04
O                     0.0000E+00           1.1095E-04
O2                    1.7618E-01           3.4979E-03
OH                    0.0000E+00           1.8592E-03
H2O                   0.0000E+00           1.7202E-01
HO2                   0.0000E+00           2.9753E-07
H2O2                  0.0000E+00           2.9732E-08
C                     0.0000E+00           2.8647E-18
CH                    0.0000E+00           4.4943E-19
CH2                   0.0000E+00           1.6274E-18
CH2SING               0.0000E+00           9.1466E-20
CH3                   0.0000E+00           1.3712E-17
CH4                   8.8090E-02           8.4254E-18
CO                    0.0000E+00           5.6217E-03
CO2                   0.0000E+00           8.2060E-02
HCO                   0.0000E+00           2.9246E-10
CH2O                  0.0000E+00           5.3288E-12
CH2OH                 0.0000E+00           1.0970E-17
CH3O                  0.0000E+00           1.6464E-19
```

CH3OH	0.0000E+00	1.1080E-18
C2H	0.0000E+00	2.9448E-25
C2H2	0.0000E+00	1.1818E-22
C2H3	0.0000E+00	6.2928E-28
C2H4	0.0000E+00	8.7924E-28
C2H5	0.0000E+00	6.7118E-33
C2H6	0.0000E+00	3.7955E-38
HCCO	0.0000E+00	8.3937E-21
CH2CO	0.0000E+00	1.4154E-20
HCCOH	0.0000E+00	1.0565E-23
N2	7.3573E-01	7.3232E-01
AR	0.0000E+00	0.0000E+00
H2CCCH	0.0000E+00	0.0000E+00
C4H2	0.0000E+00	0.0000E+00
C3H2	0.0000E+00	2.0673E-38
HCCHCCH	0.0000E+00	0.0000E+00
HF	0.0000E+00	0.0000E+00
F	0.0000E+00	0.0000E+00
CH3F	0.0000E+00	0.0000E+00
CH2F2	0.0000E+00	0.0000E+00
CHF3	0.0000E+00	0.0000E+00
CF4	0.0000E+00	0.0000E+00
CH2F	0.0000E+00	0.0000E+00
CHF2	0.0000E+00	0.0000E+00
CF3	0.0000E+00	0.0000E+00
CHF	0.0000E+00	0.0000E+00
CF2	0.0000E+00	0.0000E+00
CF	0.0000E+00	0.0000E+00
CF3O	0.0000E+00	0.0000E+00
CHF:O	0.0000E+00	0.0000E+00
CF2:O	0.0000E+00	0.0000E+00
CF:O	0.0000E+00	0.0000E+00
CF2CO	0.0000E+00	0.0000E+00
FCCO-E	0.0000E+00	0.0000E+00
CH3-CF2	0.0000E+00	0.0000E+00
CHF2-CH2	0.0000E+00	0.0000E+00
CH2:CF2	0.0000E+00	0.0000E+00
CH2:CHF	0.0000E+00	0.0000E+00
CF2:CH	0.0000E+00	0.0000E+00
C2HF	0.0000E+00	0.0000E+00
CF3-CF3	0.0000E+00	0.0000E+00
BR	0.0000E+00	0.0000E+00
BR2	0.0000E+00	0.0000E+00
HBR	0.0000E+00	0.0000E+00
CF3BR	0.0000E+00	0.0000E+00
CH3BR	0.0000E+00	0.0000E+00
CH2:CHBR	0.0000E+00	0.0000E+00
CH3-CH2BR	0.0000E+00	0.0000E+00
C2H3BR	0.0000E+00	0.0000E+00
C2H5BR	0.0000E+00	0.0000E+00
FBR	0.0000E+00	0.0000E+00
BRO	0.0000E+00	0.0000E+00
HOBR	0.0000E+00	0.0000E+00

SAMPLE 3 8% CF_3H Addition

```
 CKLIB:  Chemical Kinetics Library
         CHEMKIN-II Version 4.1, February 1993
         DOUBLE PRECISION

          KEYWORD INPUT

CONH
CONP
REAC O2      1.
REAC N2      3.76
REAC CH4     0.397
REAC CHF3    0.414
REAC CF3BR   0.
TEMP   298.
PRES   1.
END

 Constant pressure and enthalpy problem:

EQUIL:  Chemkin interface for Stanjan-III
        CHEMKIN-II Version 3.0, December 1992
        DOUBLE PRECISION

        WORKING SPACE REQUIREMENTS
            PROVIDED          REQUIRED
INTEGER             5000              2387
REAL                5000              4119
 STANJAN:  Version 3.8C, May 1988
           W. C. Reynolds, Stanford Univ.

                    INITIAL STATE:       EQUILIBRIUM STATE:
P (atm)               1.0000E+00           1.0000E+00
T (K)                 2.9800E+02           2.1460E+03
V (cm3/gm)            7.8884E+02           6.3450E+03
H (erg/gm)           -1.8428E+10          -1.8428E+10
U (erg/gm)           -1.9228E+10          -2.4857E+10
S (erg/gm-K)          6.6641E+07           9.6505E+07
W (gm/mole)           3.0997E+01           2.7753E+01


Mole Fractions
H2                    0.0000E+00           7.6964E-04
H                     0.0000E+00           1.1437E-04
O                     0.0000E+00           1.1903E-04
O2                    1.7950E-01           3.9195E-03
OH                    0.0000E+00           1.1365E-03
H2O                   0.0000E+00           5.9688E-02
HO2                   0.0000E+00           1.9223E-07
H2O2                  0.0000E+00           1.0984E-08
C                     0.0000E+00           4.0404E-18
CH                    0.0000E+00           3.6295E-19
CH2                   0.0000E+00           7.4906E-19
CH2SING               0.0000E+00           4.2182E-20
CH3                   0.0000E+00           3.5907E-18
CH4                   7.1262E-02           1.2569E-18
CO                    0.0000E+00           8.0320E-03
CO2                   0.0000E+00           1.2231E-01
HCO                   0.0000E+00           2.4274E-10
CH2O                  0.0000E+00           2.5287E-12
CH2OH                 0.0000E+00           3.0152E-18
CH3O                  0.0000E+00           4.5325E-20
```

CH3OH	0.0000E+00	1.7375E-19
C2H	0.0000E+00	3.2247E-25
C2H2	0.0000E+00	7.3266E-23
C2H3	0.0000E+00	2.2560E-28
C2H4	0.0000E+00	1.7930E-28
C2H5	0.0000E+00	6.1152E-38
C2H6	0.0000E+00	0.0000E+00
HCCO	0.0000E+00	9.5308E-21
CH2CO	0.0000E+00	9.1534E-21
HCCOH	0.0000E+00	6.8801E-24
N2	6.7492E-01	6.0430E-01
AR	0.0000E+00	0.0000E+00
H2CCCH	0.0000E+00	0.0000E+00
C4H2	0.0000E+00	0.0000E+00
C3H2	0.0000E+00	1.5812E-38
HCCHCCH	0.0000E+00	0.0000E+00
HF	0.0000E+00	1.9959E-01
F	0.0000E+00	2.1678E-05
CH3F	0.0000E+00	4.2922E-19
CH2F2	0.0000E+00	1.1501E-18
CHF3	7.4313E-02	5.9315E-18
CF4	0.0000E+00	5.0559E-18
CH2F	0.0000E+00	5.6739E-18
CHF2	0.0000E+00	9.1268E-18
CF3	0.0000E+00	7.0640E-18
CHF	0.0000E+00	3.2650E-17
CF2	0.0000E+00	6.4250E-15
CF	0.0000E+00	1.3574E-15
CF3O	0.0000E+00	2.5142E-20
CHF:O	0.0000E+00	2.0143E-10
CF2:O	0.0000E+00	1.9436E-09
CF:O	0.0000E+00	4.8100E-10
CF2CO	0.0000E+00	1.6557E-24
FCCO-E	0.0000E+00	2.0781E-22
CH3-CF2	0.0000E+00	2.3838E-33
CHF2-CH2	0.0000E+00	1.5041E-33
CH2:CF2	0.0000E+00	1.3909E-28
CH2:CHF	0.0000E+00	1.4063E-27
CF2:CH	0.0000E+00	3.8237E-29
C2HF	0.0000E+00	7.5216E-25
CF3-CF3	0.0000E+00	0.0000E+00
BR	0.0000E+00	0.0000E+00
BR2	0.0000E+00	0.0000E+00
HBR	0.0000E+00	0.0000E+00
CF3BR	0.0000E+00	0.0000E+00
CH3BR	0.0000E+00	0.0000E+00
CH2:CHBR	0.0000E+00	0.0000E+00
CH3-CH2BR	0.0000E+00	0.0000E+00
C2H3BR	0.0000E+00	0.0000E+00
C2H5BR	0.0000E+00	0.0000E+00
FBR	0.0000E+00	0.0000E+00
BRO	0.0000E+00	0.0000E+00
HOBR	0.0000E+00	0.0000E+00

SAMPLE 4 8% CF_3H Addition with 21% O_2 Conentration

```
 CKLIB:  Chemical Kinetics Library
         CHEMKIN-II Version 4.1, February 1993
         DOUBLE PRECISION

          KEYWORD INPUT

CONH
CONP
REAC O2      1.
REAC N2      3.381
REAC CH4     0.405
REAC CHF3    0.381
REAC CF3BR   0.
TEMP   298.
PRES   1.
END

 Constant pressure and enthalpy problem:

 EQUIL:  Chemkin interface for Stanjan-III
         CHEMKIN-II Version 3.0, December 1992
         DOUBLE PRECISION

         WORKING SPACE REQUIREMENTS
             PROVIDED          REQUIRED
INTEGER              5000              2387
REAL                 5000              4119
  STANJAN:  Version 3.8C, May 1988
            W. C. Reynolds, Stanford Univ.

                    INITIAL STATE:       EQUILIBRIUM STATE:
P (atm)               1.0000E+00           1.0000E+00
T (K)                 2.9800E+02           2.2255E+03
V (cm3/gm)            7.9021E+02           6.6021E+03
H (erg/gm)           -1.8502E+10          -1.8502E+10
U (erg/gm)           -1.9303E+10          -2.5191E+10
S (erg/gm-K)          6.6880E+07           9.7664E+07
W (gm/mole)           3.0943E+01           2.7660E+01


Mole Fractions
H2                    0.0000E+00           1.2584E-03
H                     0.0000E+00           2.3058E-04
O                     0.0000E+00           2.4197E-04
O2                    1.9354E-01           5.8225E-03
OH                    0.0000E+00           1.9067E-03
H2O                   0.0000E+00           7.1907E-02
HO2                   0.0000E+00           3.7153E-07
H2O2                  0.0000E+00           2.0131E-08
C                     0.0000E+00           2.5640E-17
CH                    0.0000E+00           2.2970E-18
CH2                   0.0000E+00           3.9691E-18
CH2SING               0.0000E+00           2.4060E-19
CH3                   0.0000E+00           1.4858E-17
CH4                   7.8382E-02           4.2806E-18
CO                    0.0000E+00           1.1657E-02
CO2                   0.0000E+00           1.2432E-01
HCO                   0.0000E+00           6.0964E-10
CH2O                  0.0000E+00           5.9823E-12
CH2OH                 0.0000E+00           1.1027E-17
CH3O                  0.0000E+00           1.7627E-19
```

CH3OH	0.0000E+00	5.5349E-19
C2H	0.0000E+00	2.9009E-24
C2H2	0.0000E+00	4.2722E-22
C2H3	0.0000E+00	1.9113E-27
C2H4	0.0000E+00	1.1803E-27
C2H5	0.0000E+00	7.5697E-33
C2H6	0.0000E+00	0.0000E+00
HCCO	0.0000E+00	4.7604E-20
CH2CO	0.0000E+00	3.7262E-20
HCCOH	0.0000E+00	3.6547E-23
N2	6.5434E-01	5.8491E-01
AR	0.0000E+00	0.0000E+00
H2CCCH	0.0000E+00	0.0000E+00
C4H2	0.0000E+00	0.0000E+00
C3H2	0.0000E+00	1.3869E-33
HCCHCCH	0.0000E+00	0.0000E+00
HF	0.0000E+00	1.9770E-01
F	0.0000E+00	3.4666E-05
CH3F	0.0000E+00	1.1152E-18
CH2F2	0.0000E+00	2.0667E-18
CHF3	7.3737E-02	6.9673E-18
CF4	0.0000E+00	3.9703E-18
CH2F	0.0000E+00	1.7432E-17
CHF2	0.0000E+00	1.9344E-17
CF3	0.0000E+00	1.0237E-17
CHF	0.0000E+00	1.0711E-16
CF2	0.0000E+00	1.2124E-14
CF	0.0000E+00	4.5584E-15
CF3O	0.0000E+00	3.1956E-20
CHF:O	0.0000E+00	2.9682E-10
CF2:O	0.0000E+00	1.8084E-09
CF:O	0.0000E+00	8.3581E-10
CF2CO	0.0000E+00	4.7154E-24
FCCO-E	0.0000E+00	9.3262E-22
CH3-CF2	0.0000E+00	1.1201E-32
CHF2-CH2	0.0000E+00	7.4245E-33
CH2:CF2	0.0000E+00	4.7974E-28
CH2:CHF	0.0000E+00	6.7281E-27
CF2:CH	0.0000E+00	1.7779E-28
C2HF	0.0000E+00	3.7933E-24
CF3-CF3	0.0000E+00	0.0000E+00
BR	0.0000E+00	0.0000E+00
BR2	0.0000E+00	0.0000E+00
HBR	0.0000E+00	0.0000E+00
CF3BR	0.0000E+00	0.0000E+00
CH3BR	0.0000E+00	0.0000E+00
CH2:CHBR	0.0000E+00	0.0000E+00
CH3-CH2BR	0.0000E+00	0.0000E+00
C2H3BR	0.0000E+00	0.0000E+00
C2H5BR	0.0000E+00	0.0000E+00
FBR	0.0000E+00	0.0000E+00
BRO	0.0000E+00	0.0000E+00
HOBR	0.0000E+00	0.0000E+00

SAMPLE 5 15% CF_3H Addition (H atom < F atom)

```
 CKLIB:  Chemical Kinetics Library
          CHEMKIN-II Version 4.1, February 1993
          DOUBLE PRECISION

           KEYWORD INPUT

 CONH
 CONP
 REAC O2      1.
 REAC N2      3.76
 REAC CH4     0.290
 REAC CHF3    0.840
 REAC CF3BR   0.
 TEMP   298.
 PRES   1.
 END

  Constant pressure and enthalpy problem:

 EQUIL:  Chemkin interface for Stanjan-III
         CHEMKIN-II Version 3.0, December 1992
         DOUBLE PRECISION

         WORKING SPACE REQUIREMENTS
             PROVIDED          REQUIRED
 INTEGER             5000              2387
 REAL                5000              4119
  STANJAN:  Version 3.8C, May 1988
            W. C. Reynolds, Stanford Univ.

                     INITIAL STATE:       EQUILIBRIUM STATE:
 P (atm)                1.0000E+00           1.0000E+00
 T (K)                  2.9800E+02           1.9507E+03
 V (cm3/gm)             7.1726E+02           5.5652E+03
 H (erg/gm)            -3.0240E+10          -3.0240E+10
 U (erg/gm)            -3.0967E+10          -3.5879E+10
 S (erg/gm-K)           6.2094E+07           9.2239E+07
 W (gm/mole)            3.4091E+01           2.8762E+01


 Mole Fractions
 H2                     0.0000E+00           7.8599E-11
 H                      0.0000E+00           1.0224E-08
 O                      0.0000E+00           7.1409E-06
 O2                     1.6978E-01           2.4769E-04
 OH                     0.0000E+00           7.4180E-08
 H2O                    0.0000E+00           6.2794E-09
 HO2                    0.0000E+00           3.7011E-12
 H2O2                   0.0000E+00           1.5642E-16
 C                      0.0000E+00           1.2918E-19
 CH                     0.0000E+00           7.5124E-24
 CH2                    0.0000E+00           1.6101E-26
 CH2SING                0.0000E+00           7.4239E-28
 CH3                    0.0000E+00           9.7794E-29
 CH4                    4.9236E-02           3.7811E-32
 CO                     0.0000E+00           6.9003E-03
 CO2                    0.0000E+00           1.2543E-01
 HCO                    0.0000E+00           2.8584E-14
 CH2O                   0.0000E+00           2.2486E-19
 CH2OH                  0.0000E+00           5.0630E-29
 CH3O                   0.0000E+00           6.4367E-31
```

CH3OH	0.0000E+00	2.7412E-33
C2H	0.0000E+00	1.5079E-29
C2H2	0.0000E+00	6.8419E-30
C2H3	0.0000E+00	0.0000E+00
C2H4	0.0000E+00	0.0000E+00
C2H5	0.0000E+00	0.0000E+00
C2H6	0.0000E+00	0.0000E+00
HCCO	0.0000E+00	9.2295E-25
CH2CO	0.0000E+00	1.0016E-27
HCCOH	0.0000E+00	3.6232E-31
N2	6.3837E-01	5.3860E-01
AR	0.0000E+00	0.0000E+00
H2CCCH	0.0000E+00	0.0000E+00
C4H2	0.0000E+00	0.0000E+00
C3H2	0.0000E+00	0.0000E+00
HCCHCCH	0.0000E+00	0.0000E+00
HF	0.0000E+00	2.8649E-01
F	0.0000E+00	1.2796E-02
CH3F	0.0000E+00	9.4176E-26
CH2F2	0.0000E+00	2.4495E-18
CHF3	1.4261E-01	1.4378E-10
CF4	0.0000E+00	1.3102E-03
CH2F	0.0000E+00	1.2187E-21
CHF2	0.0000E+00	1.9155E-14
CF3	0.0000E+00	1.4877E-07
CHF	0.0000E+00	9.1391E-18
CF2	0.0000E+00	2.9234E-08
CF	0.0000E+00	5.5806E-13
CF3O	0.0000E+00	3.3412E-10
CHF:O	0.0000E+00	2.3321E-10
CF2:O	0.0000E+00	2.8224E-02
CF:O	0.0000E+00	5.4898E-07
CF2CO	0.0000E+00	5.8524E-18
FCCO-E	0.0000E+00	9.4790E-20
CH3-CF2	0.0000E+00	0.0000E+00
CHF2-CH2	0.0000E+00	0.0000E+00
CH2:CF2	0.0000E+00	2.6708E-28
CH2:CHF	0.0000E+00	4.2412E-36
CF2:CH	0.0000E+00	4.9877E-26
C2HF	0.0000E+00	3.5614E-25
CF3-CF3	0.0000E+00	2.8953E-13
BR	0.0000E+00	0.0000E+00
BR2	0.0000E+00	0.0000E+00
HBR	0.0000E+00	0.0000E+00
CF3BR	0.0000E+00	0.0000E+00
CH3BR	0.0000E+00	0.0000E+00
CH2:CHBR	0.0000E+00	0.0000E+00
CH3-CH2BR	0.0000E+00	0.0000E+00
C2H3BR	0.0000E+00	0.0000E+00
C2H5BR	0.0000E+00	0.0000E+00
FBR	0.0000E+00	0.0000E+00
BRO	0.0000E+00	0.0000E+00
HOBR	0.0000E+00	0.0000E+00

SAMPLE 6 3% CF_3Br Addition

```
 CKLIB:  Chemical Kinetics Library
         CHEMKIN-II Version 4.1, February 1993
         DOUBLE PRECISION

          KEYWORD INPUT

CONH
CONP
REAC O2      1.
REAC N2      3.76
REAC CH4     0.5
REAC CHF3    0.
REAC CF3BR   0.147
TEMP   298.
PRES   1.
END

 Constant pressure and enthalpy problem:

 EQUIL:  Chemkin interface for Stanjan-III
         CHEMKIN-II Version 3.0, December 1992
         DOUBLE PRECISION

         WORKING SPACE REQUIREMENTS
             PROVIDED          REQUIRED
INTEGER              5000              2387
REAL                 5000              4119
  STANJAN:  Version 3.8C, May 1988
            W. C. Reynolds, Stanford Univ.

                    INITIAL STATE:      EQUILIBRIUM STATE:
P (atm)               1.0000E+00          1.0000E+00
T (K)                 2.9800E+02          2.1696E+03
V (cm3/gm)            7.9054E+02          6.1370E+03
H (erg/gm)           -7.9357E+09         -7.9357E+09
U (erg/gm)           -8.7368E+09         -1.4154E+10
S (erg/gm-K)          6.5878E+07          9.3161E+07
W (gm/mole)           3.0930E+01          2.9009E+01


Mole Fractions
H2                    0.0000E+00          2.5450E-03
H                     0.0000E+00          2.3891E-04
O                     0.0000E+00          1.0427E-04
O2                    1.8495E-01          2.2022E-03
OH                    0.0000E+00          1.5843E-03
H2O                   0.0000E+00          1.2691E-01
HO2                   0.0000E+00          1.9744E-07
H2O2                  0.0000E+00          1.8729E-08
C                     0.0000E+00          1.1785E-17
CH                    0.0000E+00          1.7846E-18
CH2                   0.0000E+00          5.8871E-18
CH2SING               0.0000E+00          3.3904E-19
CH3                   0.0000E+00          4.4155E-17
CH4                   9.2473E-02          2.4570E-17
CO                    0.0000E+00          1.0548E-02
CO2                   0.0000E+00          1.0168E-01
HCO                   0.0000E+00          6.3561E-10
CH2O                  0.0000E+00          1.0969E-11
CH2OH                 0.0000E+00          2.5199E-17
CH3O                  0.0000E+00          3.8594E-19
```

CH3OH	0.0000E+00	2.3489E-18
C2H	0.0000E+00	2.9314E-24
C2H2	0.0000E+00	9.8463E-22
C2H3	0.0000E+00	5.7320E-27
C2H4	0.0000E+00	7.1171E-27
C2H5	0.0000E+00	5.9395E-32
C2H6	0.0000E+00	4.8110E-33
HCCO	0.0000E+00	5.1111E-20
CH2CO	0.0000E+00	7.7810E-20
HCCOH	0.0000E+00	6.3421E-23
N2	6.9539E-01	6.5221E-01
AR	0.0000E+00	0.0000E+00
H2CCCH	0.0000E+00	0.0000E+00
C4H2	0.0000E+00	0.0000E+00
C3H2	0.0000E+00	2.9279E-33
HCCHCCH	0.0000E+00	0.0000E+00
HF	0.0000E+00	7.6490E-02
F	0.0000E+00	5.6972E-06
CH3F	0.0000E+00	1.0433E-18
CH2F2	0.0000E+00	3.3733E-19
CHF3	0.0000E+00	2.0634E-19
CF4	0.0000E+00	2.1004E-20
CH2F	0.0000E+00	8.6030E-18
CHF2	0.0000E+00	1.6685E-18
CF3	0.0000E+00	1.5528E-19
CHF	0.0000E+00	2.9935E-17
CF2	0.0000E+00	6.7201E-16
CF	0.0000E+00	7.4291E-16
CF3O	0.0000E+00	3.7477E-22
CHF:O	0.0000E+00	1.0212E-10
CF2:O	0.0000E+00	1.1565E-10
CF:O	0.0000E+00	1.5199E-10
CF2CO	0.0000E+00	2.3009E-25
FCCO-E	0.0000E+00	1.4558E-22
CH3-CF2	0.0000E+00	2.6259E-33
CHF2-CH2	0.0000E+00	1.6820E-33
CH2:CF2	0.0000E+00	8.2648E-29
CH2:CHF	0.0000E+00	6.8385E-27
CF2:CH	0.0000E+00	1.4750E-29
C2HF	0.0000E+00	1.3057E-24
CF3-CF3	0.0000E+00	0.0000E+00
BR	0.0000E+00	1.5764E-02
BR2	0.0000E+00	1.9435E-05
HBR	0.0000E+00	9.6898E-03
CF3BR	2.7187E-02	1.2076E-21
CH3BR	0.0000E+00	1.4314E-18
CH2:CHBR	0.0000E+00	7.9704E-28
CH3-CH2BR	0.0000E+00	1.0808E-33
C2H3BR	0.0000E+00	7.9704E-28
C2H5BR	0.0000E+00	1.0808E-33
FBR	0.0000E+00	1.1974E-07
BRO	0.0000E+00	1.7090E-06
HOBR	0.0000E+00	3.7205E-06

SAMPLE 7 CO/CH_4 Fuel, Uninhibited

```
 CKLIB:  Chemical Kinetics Library
         CHEMKIN-II Version 4.1, February 1993
         DOUBLE PRECISION

          KEYWORD INPUT

CONH
CONP
REAC O2      1.
REAC N2      3.76
REAC CO      1.923
REAC CH4     0.019
REAC CHF3    0.
REAC CF3BR   0.
TEMP   298.
PRES   1.
END

 Constant pressure and enthalpy problem:

 EQUIL:  Chemkin interface for Stanjan-III
         CHEMKIN-II Version 3.0, December 1992
         DOUBLE PRECISION

         WORKING SPACE REQUIREMENTS
             PROVIDED        REQUIRED
INTEGER              5000            2387
REAL                 5000            4119
 STANJAN:  Version 3.8C, May 1988
           W. C. Reynolds, Stanford Univ.

                    INITIAL STATE:      EQUILIBRIUM STATE:
P (atm)               1.0000E+00          1.0000E+00
T (K)                 2.9800E+02          2.3856E+03
V (cm3/gm)            8.5575E+02          5.9960E+03
H (erg/gm)           -1.1174E+10         -1.1174E+10
U (erg/gm)           -1.2041E+10         -1.7249E+10
S (erg/gm-K)          7.1200E+07          8.7092E+07
W (gm/mole)           2.8573E+01          3.2648E+01


Mole Fractions
H2                    0.0000E+00          1.3344E-04
H                     0.0000E+00          1.7165E-04
O                     0.0000E+00          1.1218E-03
O2                    1.4921E-01          1.9560E-02
OH                    0.0000E+00          1.2999E-03
H2O                   0.0000E+00          5.6090E-03
HO2                   0.0000E+00          4.1961E-07
H2O2                  0.0000E+00          4.3068E-09
C                     0.0000E+00          1.0130E-15
CH                    0.0000E+00          1.8825E-17
CH2                   0.0000E+00          4.9041E-18
CH2SING               0.0000E+00          3.3981E-19
CH3                   0.0000E+00          2.4482E-18
CH4                   2.8350E-03          1.0382E-19
CO                    2.8693E-01          4.0502E-02
CO2                   0.0000E+00          2.9058E-01
HCO                   0.0000E+00          1.1943E-09
CH2O                  0.0000E+00          2.1966E-12
CH2OH                 0.0000E+00          1.8603E-18
```

CH3O	0.0000E+00	3.3309E-20
CH3OH	0.0000E+00	1.5183E-20
C2H	0.0000E+00	6.2437E-23
C2H2	0.0000E+00	8.7179E-22
C2H3	0.0000E+00	1.6015E-27
C2H4	0.0000E+00	1.3062E-28
C2H5	0.0000E+00	3.7704E-37
C2H6	0.0000E+00	0.0000E+00
HCCO	0.0000E+00	4.4940E-19
CH2CO	0.0000E+00	5.0699E-20
HCCOH	0.0000E+00	8.0703E-23
N2	5.6103E-01	6.4102E-01
AR	0.0000E+00	0.0000E+00
H2CCCH	0.0000E+00	7.5423E-37
C4H2	0.0000E+00	0.0000E+00
C3H2	0.0000E+00	1.8671E-32
HCCHCCH	0.0000E+00	0.0000E+00
HF	0.0000E+00	0.0000E+00
F	0.0000E+00	0.0000E+00
CH3F	0.0000E+00	0.0000E+00
CH2F2	0.0000E+00	0.0000E+00
CHF3	0.0000E+00	0.0000E+00
CF4	0.0000E+00	0.0000E+00
CH2F	0.0000E+00	0.0000E+00
CHF2	0.0000E+00	0.0000E+00
CF3	0.0000E+00	0.0000E+00
CHF	0.0000E+00	0.0000E+00
CF2	0.0000E+00	0.0000E+00
CF	0.0000E+00	0.0000E+00
CF3O	0.0000E+00	0.0000E+00
CHF:O	0.0000E+00	0.0000E+00
CF2:O	0.0000E+00	0.0000E+00
CF:O	0.0000E+00	0.0000E+00
CF2CO	0.0000E+00	0.0000E+00
FCCO-E	0.0000E+00	0.0000E+00
CH3-CF2	0.0000E+00	0.0000E+00
CHF2-CH2	0.0000E+00	0.0000E+00
CH2:CF2	0.0000E+00	0.0000E+00
CH2:CHF	0.0000E+00	0.0000E+00
CF2:CH	0.0000E+00	0.0000E+00
C2HF	0.0000E+00	0.0000E+00
CF3-CF3	0.0000E+00	0.0000E+00
BR	0.0000E+00	0.0000E+00
BR2	0.0000E+00	0.0000E+00
HBR	0.0000E+00	0.0000E+00
CF3BR	0.0000E+00	0.0000E+00
CH3BR	0.0000E+00	0.0000E+00
CH2:CHBR	0.0000E+00	0.0000E+00
CH3-CH2BR	0.0000E+00	0.0000E+00
C2H3BR	0.0000E+00	0.0000E+00
C2H5BR	0.0000E+00	0.0000E+00
FBR	0.0000E+00	0.0000E+00
BRO	0.0000E+00	0.0000E+00
HOBR	0.0000E+00	0.0000E+00

APPENDIX IV

Diffusion Corrected Equilibrium

A first order correction to be made to the stoichiometric equilibrium calculations, described in Appendix III, accounts for the different diffusion rate of the inhibitors compared with oxygen. Since oxygen and inhibitor are consumed at the flame, they are both diffusion from the far-field into a sink at the flame. The relative rate at which the oxygen and inhibitor are consumed, therefore, depends on the ratio of their concentrations in the far-field and the ratio of their diffusion coefficients. Since the inhibitors have lower diffusion coefficients in nitrogen than does oxygen, as shown in Table AIV.1, they are consumed more slowly at the flame. In the following equilibrium calculations, the amount of inhibitor in the reactants is reduced by the ratio of the diffusion coefficients of inhibitor to oxygen in nitrogen. The reactants entered in these calculations are shown in Table AIV.2 and equilibrium temperature and product concentrations are shown in Figures AIV.1-9. Product concentrations shown in the figures are normalized by either the amount of fuel or inhibitor in the reactants.

Table AIV.1 Diffusion ratios

Species	D* (m^2/s)	D_I/D_{O2}
O_2	2.081E-5	
CF_3H	1.286E-5	0.618
CF_3Br	1.218E-5	0.585

** In N_2 at 298 K from [34].*

Table AIV.2 Calculation parameters

Mole Fractions			Moles of Reactants			
xN_2 dil.		xO_2	O_2	N_2	CH_4	
0		0.21	1	3.762	0.5	
0.02		0.2058	1	3.859	0.5	
0.04		0.2016	1	3.960	0.5	
0.06		0.1974	1	4.066	0.5	
0.08		0.1932	1	4.176	0.5	
0.1		0.1890	1	4.291	0.5	
0.12		0.1848	1	4.411	0.5	
0.14		0.1806	1	4.537	0.5	
0.16		0.1764	1	4.669	0.5	
0.18		0.1722	1	4.807	0.5	
Far-field xCF_3H	Flame xCF_3H	xO_2	O_2	N_2	CF_3H	CH_4
0	0.000	0.21	1	3.76	0.0000	0.5000
0.02	0.012	0.2074	1	3.76	0.0596	0.4851
0.04	0.025	0.2048	1	3.76	0.1206	0.4698
0.06	0.037	0.2022	1	3.76	0.1833	0.4542
0.08	0.049	0.1996	1	3.76	0.2476	0.4381
0.10	0.062	0.1970	1	3.76	0.3135	0.4216
0.12	0.074	0.1944	1	3.76	0.3813	0.4047
0.14	0.087	0.1918	1	3.76	0.4508	0.3873
0.15	0.093	0.1905	1	3.76	0.4863	0.3784
0.16	0.099	0.1892	1	3.76	0.5223	0.3694
0.18	0.111	0.1866	1	3.76	0.5958	0.3511
Far-field xCF_3Br	Flame xCF_3Br	xO_2	O_2	N_2	CF_3Br	CH_4
0	0	0.21	1	3.76	0.0000	0.5
0.005	0.003	0.2094	1	3.76	0.0140	0.5
0.01	0.006	0.2088	1	3.76	0.0280	0.5
0.015	0.009	0.2082	1	3.76	0.0421	0.5
0.02	0.012	0.2075	1	3.76	0.0564	0.5
0.03	0.018	0.2063	1	3.76	0.0850	0.5
0.04	0.023	0.2051	1	3.76	0.1141	0.5
0.05	0.029	0.2039	1	3.76	0.1434	0.5
0.06	0.035	0.2026	1	3.76	0.1732	0.5

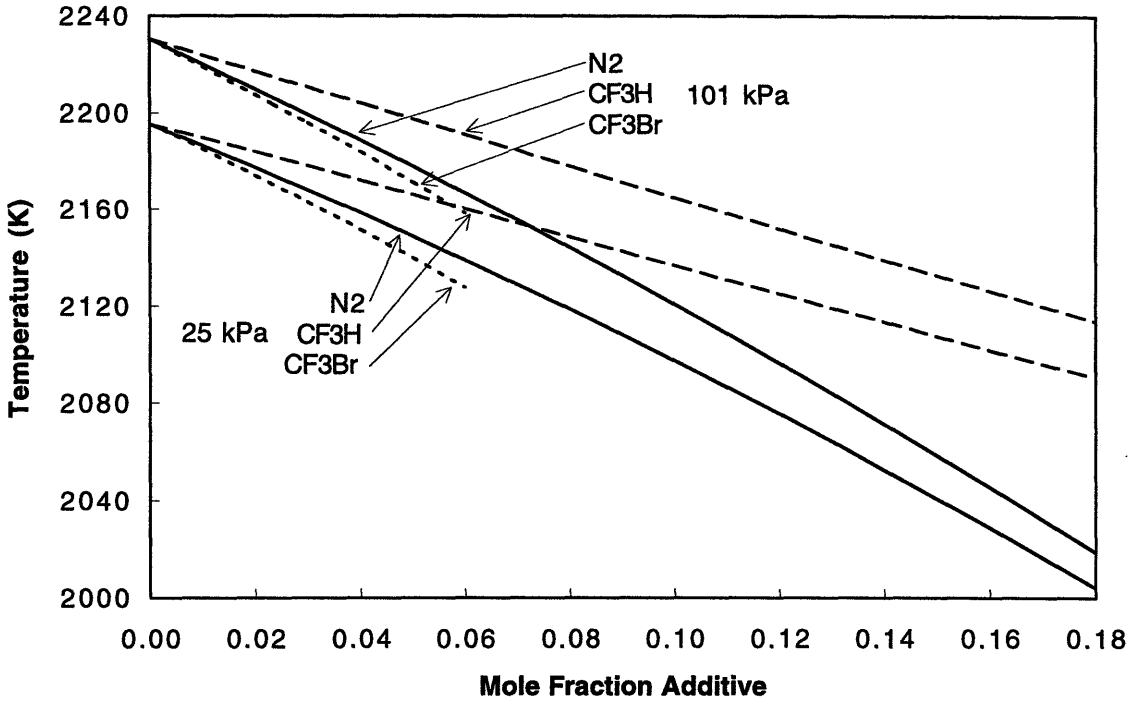

Figure AIV.1 Effect of additives (N_2, CF_3H, and CF_3Br) on equilibrium temperature. T_i = 298 K, initial mole fractions corrected for diffusion.

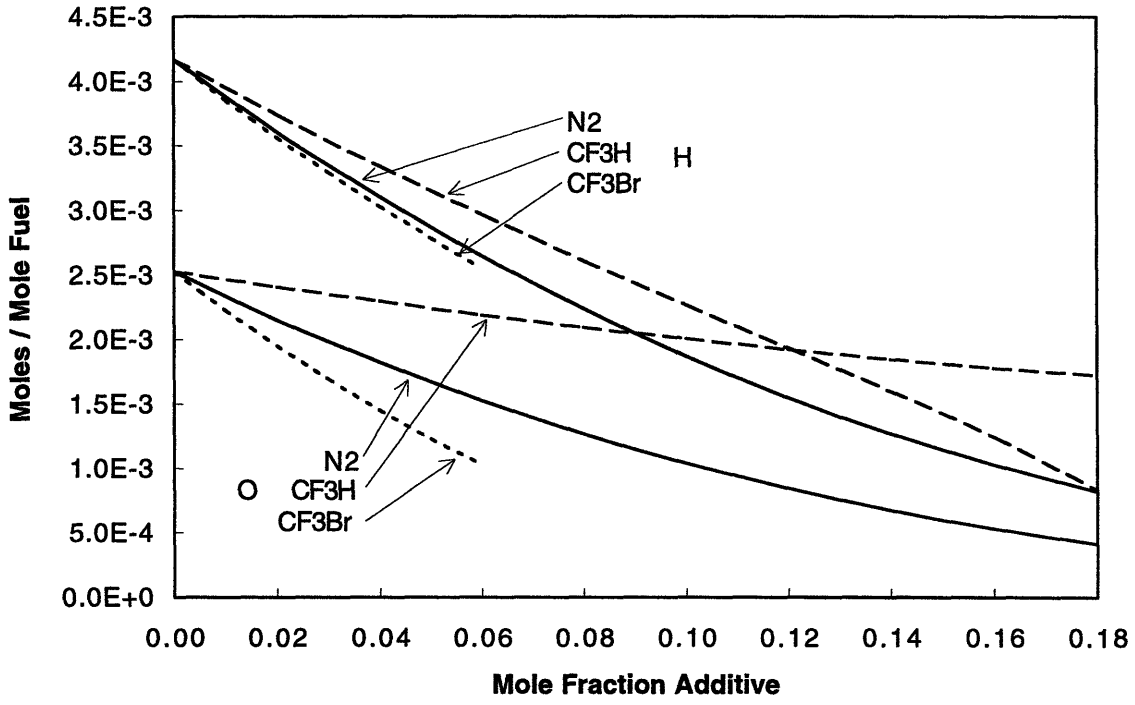

Figure AIV.2 Effect of additives on equilibrium O and H radical output. T_i = 298 K, initial mole fractions corrected for diffusion.

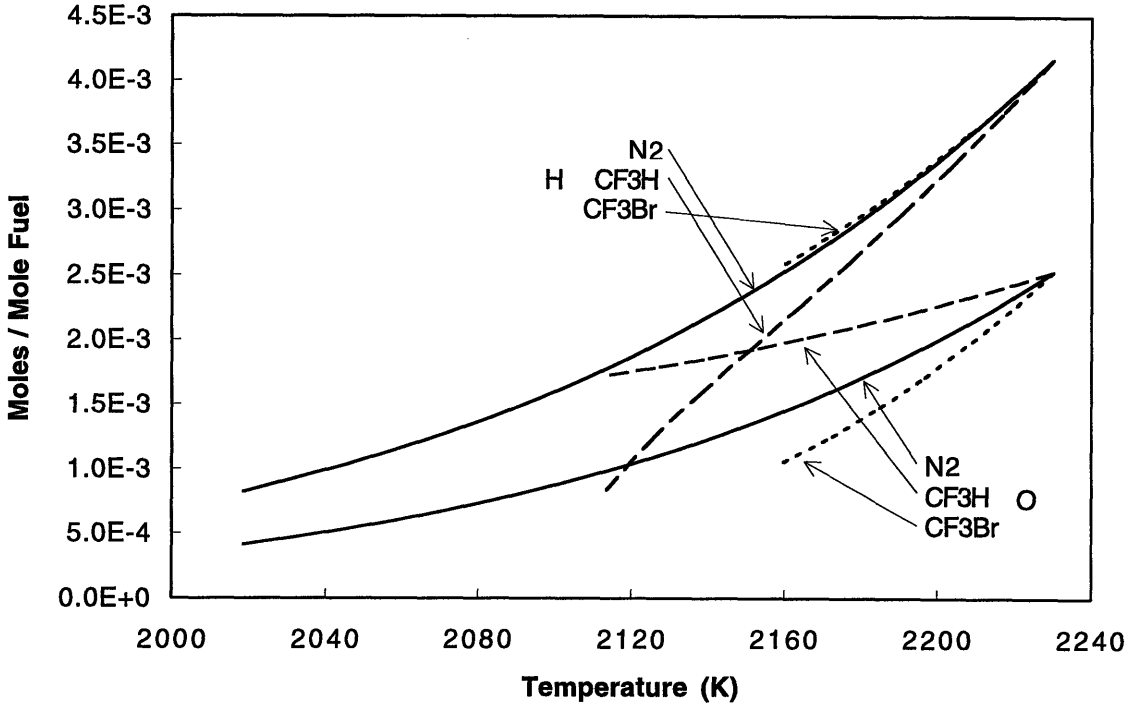

Figure AIV.3 Plot of equilibrium O and H radical output versus equilibrium temperature due to additives. T_i = 298 K, initial mole fractions corrected for diffusion.

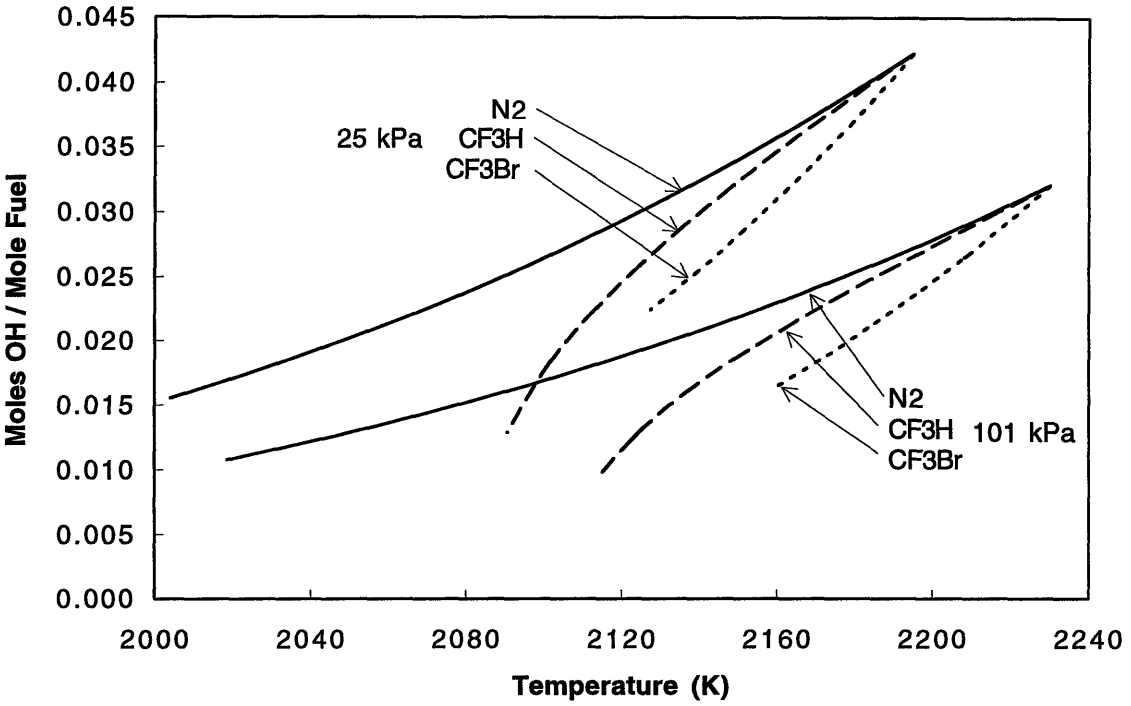

Figure AIV.4 Plot of equilibrium OH radical output versus equilibrium temperature due to additives. T_i = 298 K, initial mole fractions corrected for diffusion.

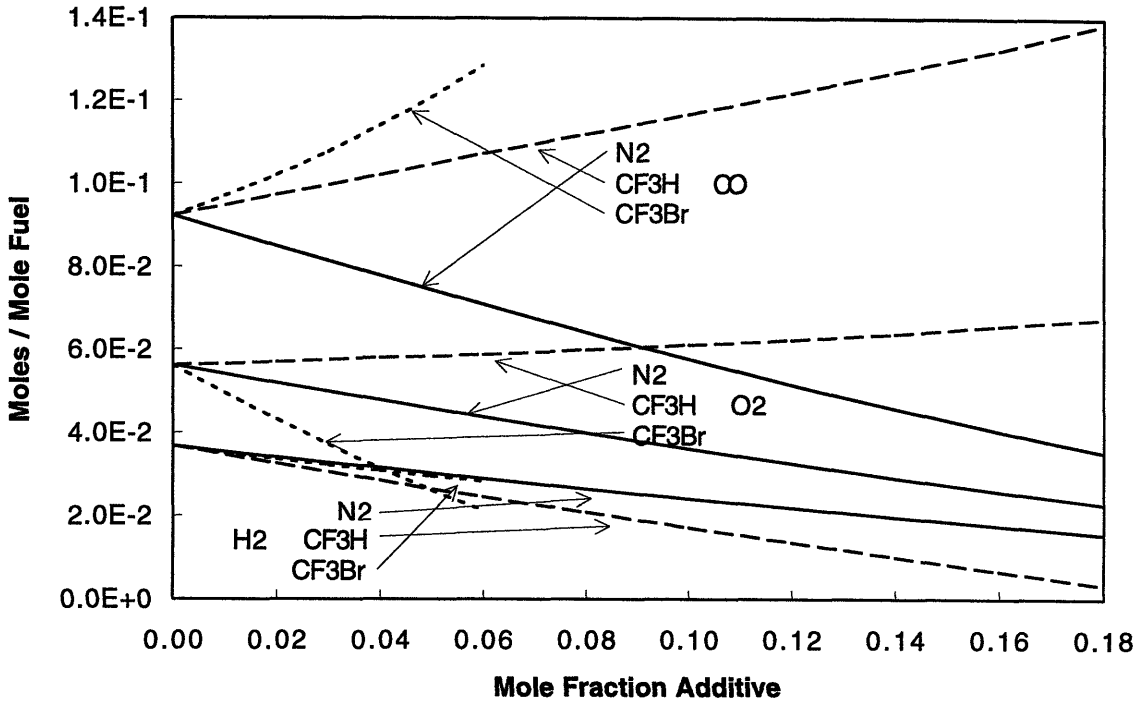

Figure AIV.5 Effect of additives on equilibrium output of CO, O_2, and H_2. T_i = 298 K, initial mole fractions corrected for diffusion.

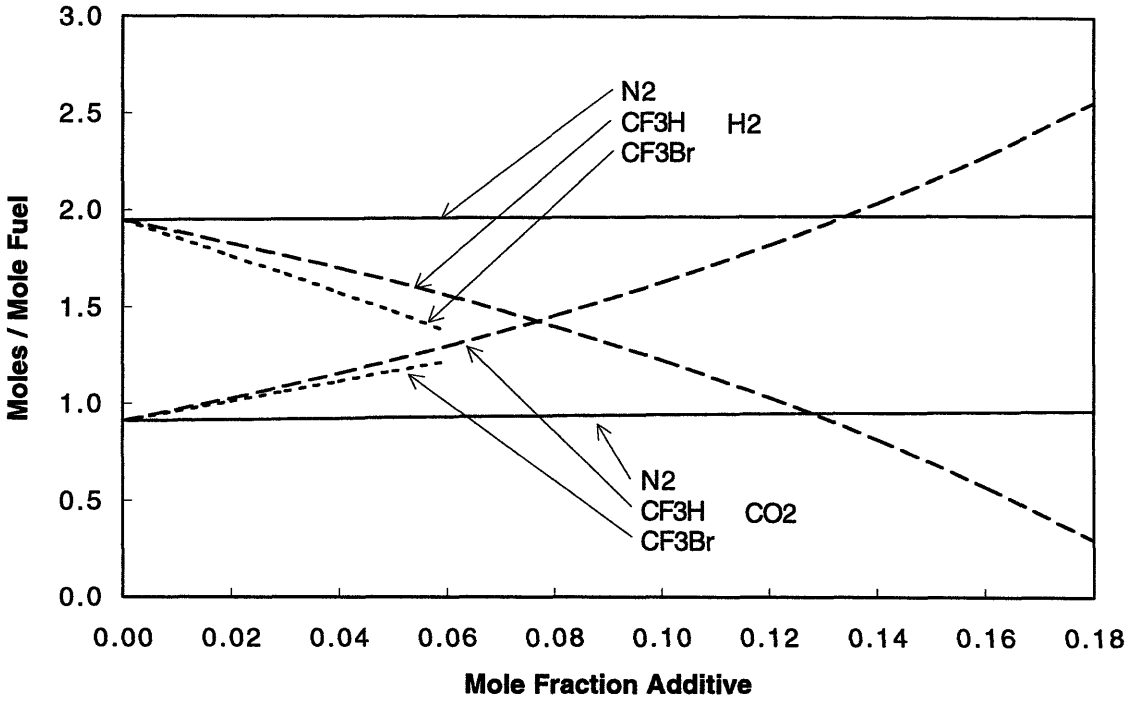

Figure AIV.6 Effect of additives on equilibrium output of H_2O and CO_2. T_i = 298 K, initial mole fractions corrected for diffusion.

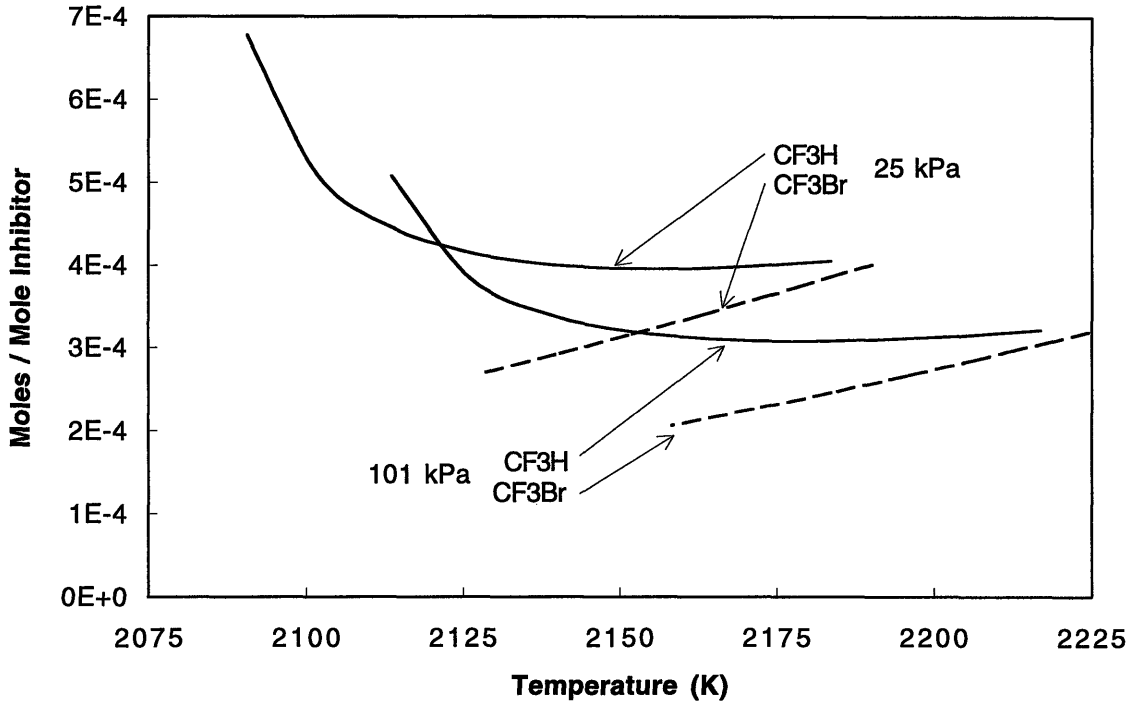

Figure AIV.7 Plot of equilibrium F radical output versus equilibrium temperature due to additives. $T_i = 298$ K, initial mole fractions corrected for diffusion.

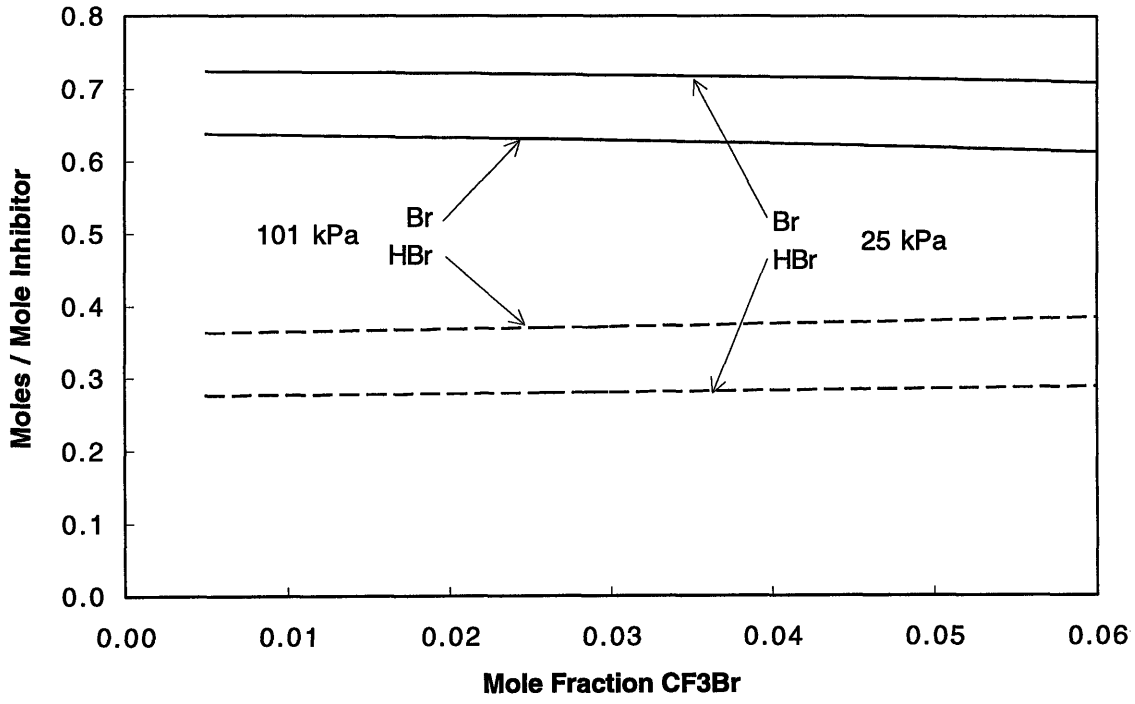

Figure AIV.8 Effect of CF_3Br addition on equilibrium Br and HBr output. $T_i = 298$ K, initial mole fractions corrected for diffusion.

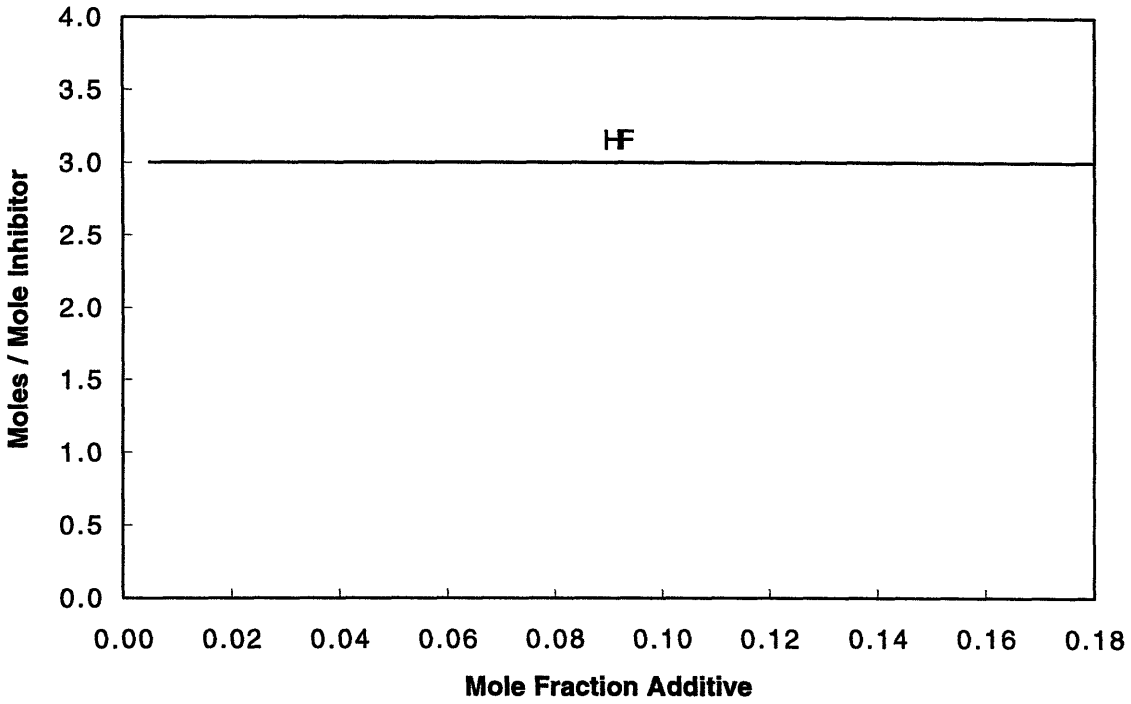

Figure AIV.9 Effect of inhibitor addition (CF_3H or CF_3Br) on equilibrium output of HF. T_i = 298 K, initial mole fractions corrected for diffusion. This shows near complete conversion of F atoms to HF.